CLOUD CHAMBER STUDIES OF COSMIC RAYS

Thesis by

James C. Fletcher

In Partial Fulfillment of the Requirements for the

Degree of Doctor of Philosophy

California Institute of Technology

Pasadena, California

1948

ABSTRACT

The large magnet and 22" diameter cloud chamber constructed by Dr. S. H. Neddermeyer and Dr. C. D. Anderson has been used in an attempt to observe mesotron disintegrations at sea level. Although no recognizable disintegrations were observed, useful data concerning energy loss of charged particles in carbon were obtained.

It was found that the present theory of energy loss of electrons first derived by Bloch and others is in very good agreement with the experimental results for the energy range 3-25 Mev. Also the results obtained provide good agreement with the theory of knock-on production by mesotrons for knock-ons whose energies lie in the range of 2-50 Mev.

It is believed that information about knock-ons of somewhat higher energies than this would be quite useful in determining some of the properties of the mesotron.

ACKNOWLEDGEMENT

The author is indebted to Professor C. D. Anderson who first suggested this problem and who rendered valuable aid during the progress of the work. He also wishes to express appreciation, at this time, for the able assistance of Mr. E. W. Cowan and of Mr. R. C. Saxena who helped work out many of the experimental details and to Mr. R. Jopson and Dr. H. K. Forster who assisted in operating the equipment during the fall of 1947. This work was supported, in part, by a contract with the Office of Naval Research; and also by a fellowship grant to the author from the Eastman Kodak Company.

TABLE OF CONTENTS

LIST OF ILLUSTRATIONS

I. INTRODUCTION

Some time before the war, Professor C. D. Anderson and Dr. S. H. Neddermeyer constructed a large magnet and vertical Wilson cloud chamber to be used for Cosmic Ray Research at sea level. The mechanical construction on both was completed, but due to the urgency of war work no data were obtained. Since the war, interest has arisen in mesotron instability and it was thought that because of its size this cloud chamber would be ideally suited for studying the disintegration electrons arising from mesotrons which come to rest in the chamber. Three graphite plates 1.1 cm. thick, were horizontally placed inside the chamber to increase the probability of the mesotrons stopping, and 12" of lead were placed above to increase the number of low energy particles. (See Fig. 4 for the experimental arrangement). A discussion of the probabilities of such events occuring and of the problems involved in observing this phenomenon appears in the appendix at the end of this thesis. It is sufficient to say at this point that although 7,000 photographs were taken, with an average of about 1 graphite plate traversed per photograph, no picture was obtained that could, with any degree of certainty, be interpreted as a mesotron which disintegrated inside the illuminated area of the chamber.

It became apparent, however, after not too many photographs were studied, that because of the large amount of graphite traversed by the cosmic ray particles, an excellent opportunity was afforded to study the interaction of these particles with an element of low atomic number. Since the data from previous research on low Z elements are rather meager,

it is the major purpose of this thesis to give some of the statistics found with our cloud chamber. These data will include:

1. Statistics on the number of secondary electrons arising from close collisions of the cosmic ray particles with the orbital electrons of the carbon atoms and
2. Statistics on the energy lost by some of these particles, namely electrons, in passing through the graphite.

II. DESCRIPTION OF APPARATUS

Leon Katz has given a fairly complete description of the magnet and cloud chamber as it was originally constructed.(1) I will summarize briefly this account and in addition give a more-or-less detailed description of the significant improvements, made by myself and my associates from 1946 until the present time.

The magnet was made over from a large Poulson Arc transformer donated by the Navy to California Institute of Technology. It is wound with copper coils of sufficient length and cross section to permit 500 amperes to flow at 120 volts. To dissipate the 60 KW of power so generated, a system was devised whereby transformer oil was circulated through the windings, then pumped outside to a heat exchanger where the heat was transferred to continuously running water. The temperature of the oil on a normal operating day (ambient temperature of 30° C) rose to about 60° C.

The pole pieces were of 24" cross section with a 14" gap. between them were placed the cloud chamber and optical system for photographing

the tracks. Under these conditions the flux density was about 5,000 gauss, uniform to approximately 4% within the illuminated area of the cloud chamber, which is 22" in diameter and 2" deep.

It is pertinent to describe more fully the method of photographing the tracks since some of the difficulties in interpreting the data are due to this. Fig. 1, is a schematic drawing of the optical system. It can be seen from the diagram that because of the small gap between pole pieces, it was necessary to tilt the cameras about 45° to the perpendicular in order that they might view the entire cloud chamber. The tracks were illuminated from the side, the light passing through a cylindrical glass ring which formed the side of the cloud chamber. The effective distance from the camera lens to the center of the cloud chamber is only about 25", whereas the chamber itself is 22" in diameter. Thus, light from tracks in the portion of the chamber farthest from the camera would be scattered through a somewhat smaller angle than light from those closest to the camera. Since the scattering power of the droplets in the track changes rapidly with scattering angle, it can be seen that there will be quite a variation in the apparent density of tracks in different parts of the chamber, hence in the apparent ionization (see tracks in Fig. 2).

Also it can be seen from Fig. 1 that there exists the problem of getting a sufficient depth of focus to maintain the entire chamber in good focus on one negative. This was partially solved by inclining the film slightly from the perpendicular to the lens axis, but because of

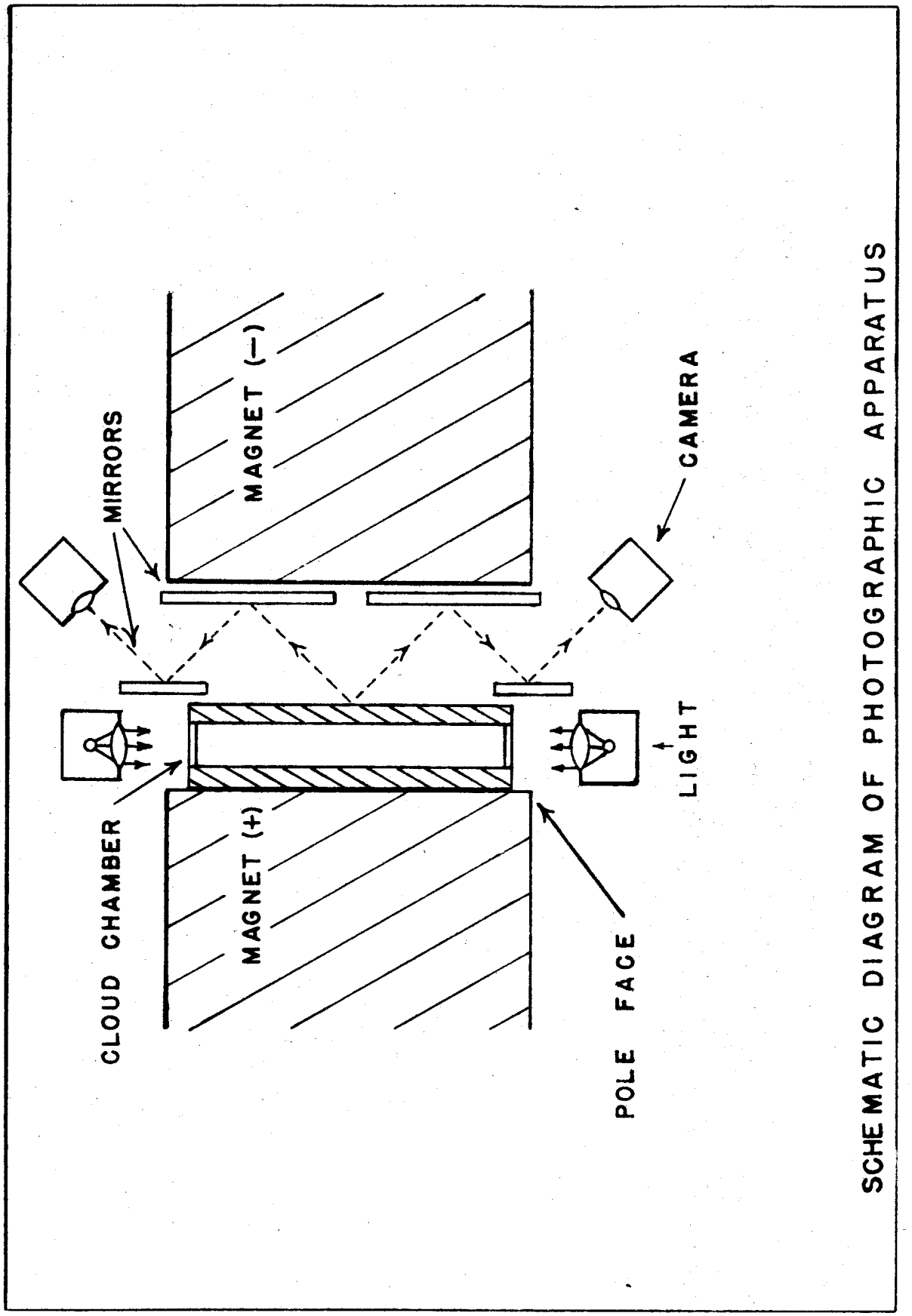
SCHEMATIC DIAGRAM OF PHOTOGRAPHIC APPARATUS
MAGNET (−)
MIRRORS
CAMERA
LIGHT
CLOUD CHAMBER
MAGNET (+)
POLE FACE

FIG. 1

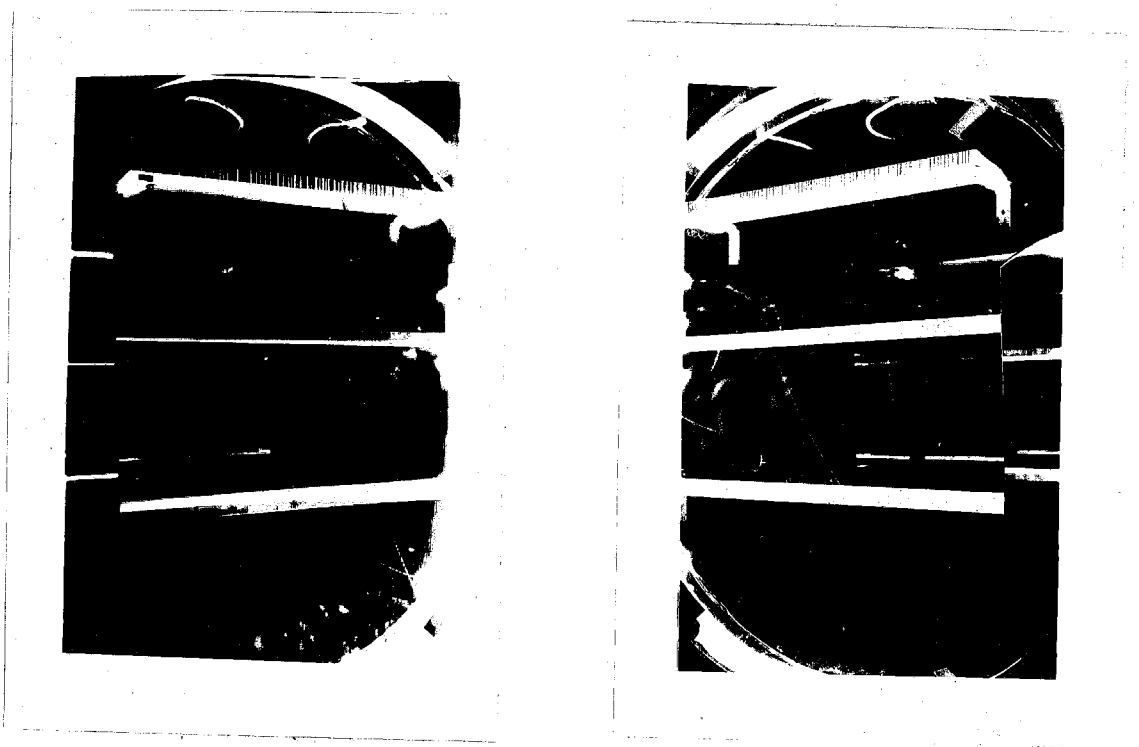

FIG. 2

An electron of 88 Mev. energy enters the bottom plate from above and loses 52 Mev. (7 times theoretical) in the graphite plate. This is a good illustration of the change in scattered light intensity from tracks in different portions of the chamber.

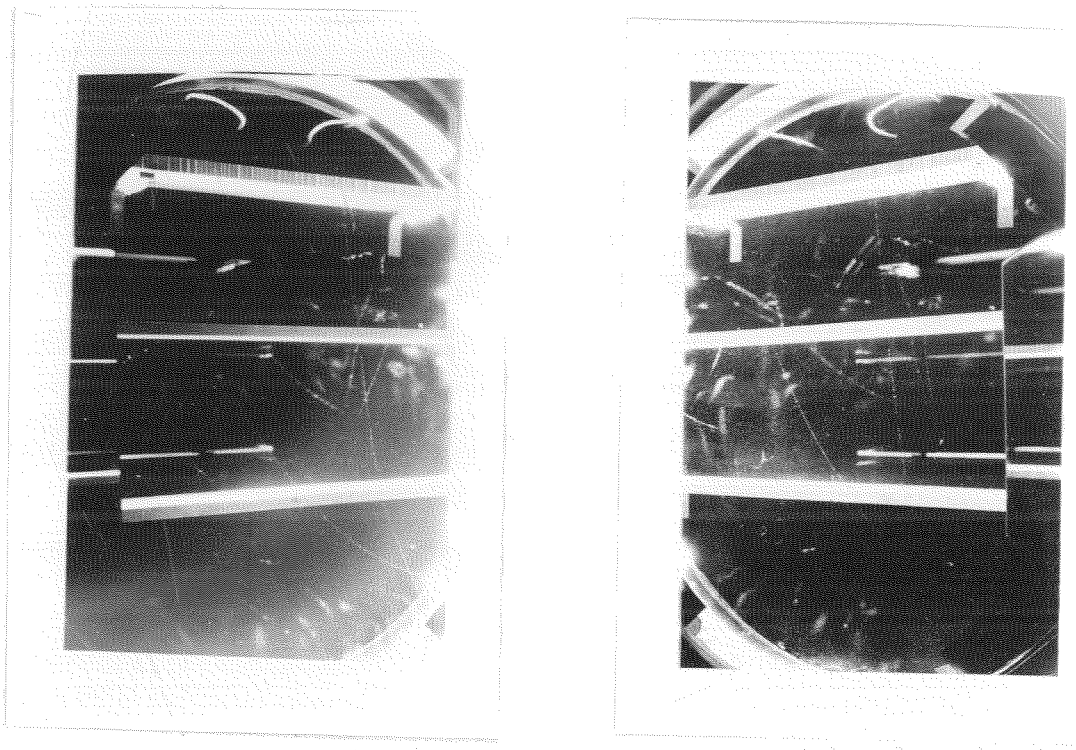

FIG. 2

An electron of 88 Mev. energy enters the bottom plate from above and loses 52 Mev. (7 times theoretical) in the graphite plate. This is a good illustration of the change in scattered light intensity from tracks in different portions of the chamber.

astigmatism inherent in any lens from rays at large angles and because of the large field of view required by the lens some of the tracks are slightly out of focus.

The problem of expanding the cloud chamber in such a small gap also presented some difficulties. Originally a piston made of 3/8" bakelite, supported by 3/32" gum rubber sheet glued to the back of the bakelite (see Fig. 3), was made to move between two stops behind the chamber by suddenly reducing the pressure behind it. The movement of the piston allowed the gas in the chamber to expand through a black velvet covering at the back of the chamber. The velvet served as a dark background for the tracks and because of its air resistance, as an "expansion equalizer" for the various parts of the chamber. This method worked well until the sheet rubber which held the bakelite in place began to pull away from the bakelite. This would allow local overexpansions to take place in the neighborhood of small air spaces trapped between rubber and bakelite. The numerous small droplets thus created would be forced through the velvet on the compression stroke of the piston causing a dense cloud to form on the next expansion. This difficulty was eliminated by removing the bakelite, the sheet rubber itself being used as the diaphragm. It was feared that contact of the rubber with the front stop might cause static charges to be generated on each expansion forming numerous droplet nucleii, so prior to the expansion the rubber was kept at a position somewhere between the stops by carefully controlling the pressure behind it. This seemed to work quite satisfactorily, giving distinct tracks without much background or fog as long as the expansion ratio was adjusted properly.

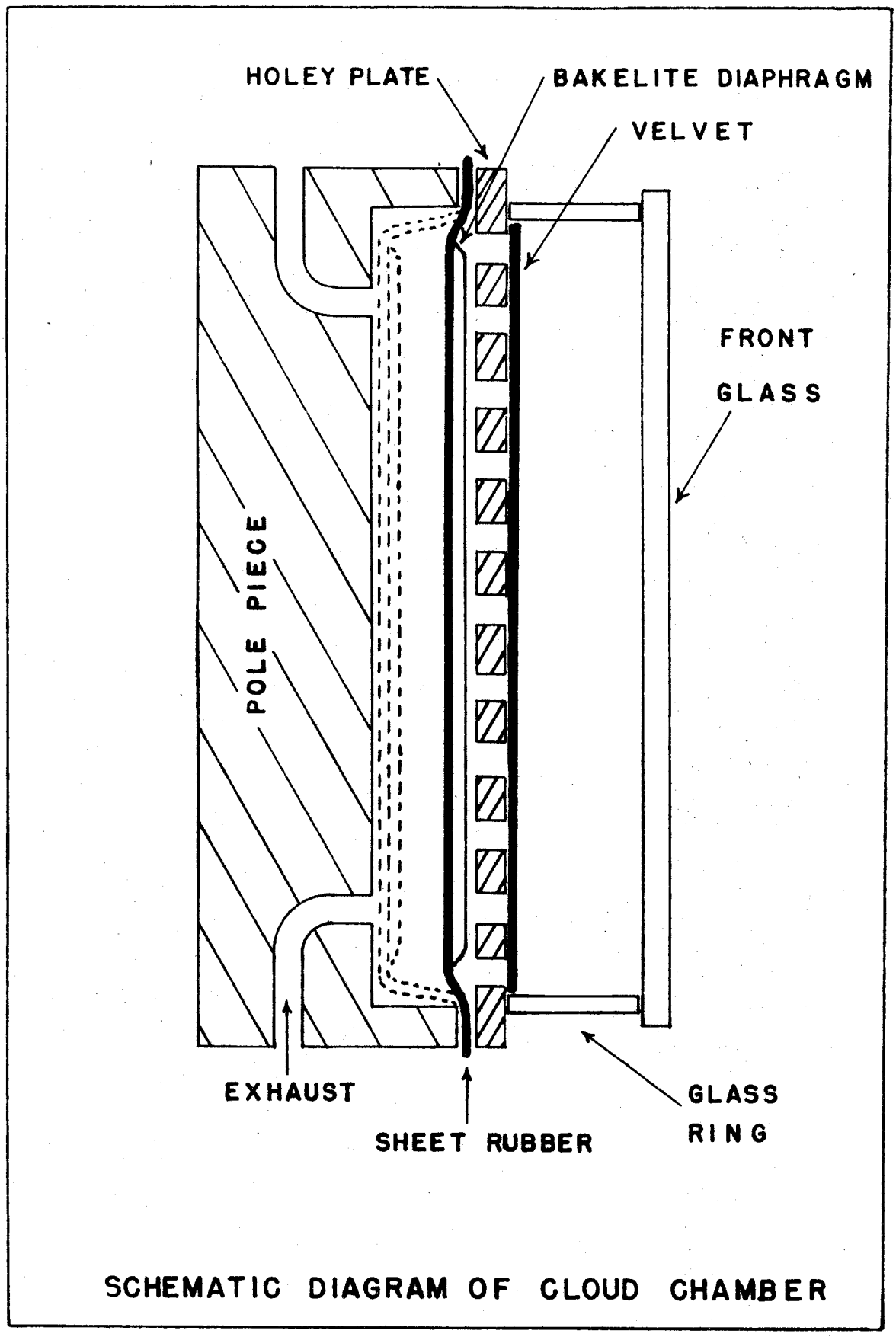

SCHEMATIC DIAGRAM OF CLOUD CHAMBER

FIG. 3

Since the area of the rubber diaphragm was 6,000 cm.^{2}, only one mm. pressure differential across the diaphragm (80 kg. of force) was sufficient to force it firmly against either stop. Hence, when the diaphragm was somewhere between stops, i.e., ready for an expansion, the pressure inside the chamber was equal to the pressure applied to the back, within one mm. Thus, the expansion ratio depended directly on this pressure (the expanded pressure, of course, depended only on the position of the back stop). The expansion ratio for an absolute ethyl alcohol - argon mixture was found to be 1.132 at 30°C. and it was found necessary to maintain this within $\pm$ .15% for distinct tracks. We have:

$$\eta = \frac{V_2}{V_1} = \frac{P_0 + P_1}{P_0 + P_2}$$

$$\frac{d\eta}{\eta} = \frac{dp_1}{P_0 + P_1}$$

η = expansion ratio

P_0 = atmospheric pressure

P_1 = pressure above atmospheric prior to expansion

P_2 = pressure above atmospheric after expansion

Since p_1 was about 22.4 cm. it is seen that dp_1 is about 3mm. pressure.

To control the pressure to this accuracy we used a manometer with off-on contacts which operated a release valve for the air behind the chamber. Air was pumped in from a "pressure-reserve" tank which was maintained at an approximately constant pressure by a standard-type

reducer valve attached to the Cal. Tech. compressed air supply. The manometer and tank combination was able to maintain the pressure to about 2 mm. when mercury was used and to less than 1 mm. when $CuSO_4$ solution (density approximately 1) was used as the manometer liquid.

However, this type of control was very sensitive to temperature changes inside the chamber. We have:

$$\frac{d\eta}{\eta} = \frac{-dp_2}{p_0 + p_2}$$

(p_1 is determined solely by the manometer regulator)

$$\text{but } p_2 + p_0 = RT$$

(neglecting the alcohol vapor pressure.)

$$\frac{dp_2}{p_2 + p_0} = \frac{dT}{T}$$

$$\frac{d\eta}{\eta} = -\frac{dT}{T}$$

Hence for T = 300°C., dT must be less than 1°C. for good tracks (actually dT turns out to be even less than this if the change in alcohol vapor-pressure is included).

Unfortunately the apparatus was housed in a non-insulated, non air-conditioned shack and as a result the temperature would change by 10°C. in a normal day's operation. No convenient means was found to allow for this variation except to monitor the apparatus and at periodic intervals (the period depending on the particular time of day) check the expansion ratio. This was a serious limitation on the number of photographs that could be taken in a day with a limited

number of operators. This, I believe, was the most serious disadvantage of this method of cloud-chamber operation.

Because of the high temperature of the magnet and because the cloud chamber is in good thermal contact with one pole piece, it was found necessary to cool the pole face independently of the rest of the magnet. This was done by allowing tap water to circulate through it. Although this procedure kept the pole face cool, it was not always at the same temperature as the surrounding air, hence large gradients often occurred between front and back of the chamber.

Also, it was found that large gradients would occur vertically across the chamber due to temperature differences between floor and roof of the shack. Often this would be 2 or 3 degrees C. just across the 2 feet of the cloud chamber. This was reduced to about $\frac{1}{2}^{o}$C. by enclosing the chamber and air gap in a wooden cabin and circulating the air inside vigorously with a large fan. The cabin also served to prevent the temperature of the cloud chamber fron changing too rapidly. At certain times of day the shack temperature might change as much as 10^{o}C. in 1 hour whereas it would take the cloud chamber 6 or 7 hours to change the same amount. Even with these precautions, however, temperature gradients caused convection currents inside the cloud chamber which produced serious distortions in the tracks.

The three graphite plates which were placed in the chamber were roughly 1.1 cm. thick, and had a density of 1.7. Before the plates were inserted into the cloud chamber it was observed that most of the distortion of the tracks occurred at the top and bottom of the chamber

and in a direction which indicated that the motion of the gas was parallel to the sides of the chamber (i.e., the glass ring). With the plates inside, the distortion was similar but occurring above and below each plate in opposite directions on the opposite sides of the plate. Thus, distortion was made much worse by adding the plates and in addition it occurred in the most interesting portions of the chamber -- near the plates. The apparent magnitude of the distortion was increased because of the angle of photography.* but this was decreased to a certain extent after the photographs were re-projected (see Section IV).

In order to clear the chamber of ions from old tracks prior to an expansion, the top and bottom plates were placed at 250 volts positive potential. This potential was removed as soon as the cosmic ray particle tripped a Geiger counter coincidence circuit. Because of the large volume of the chamber and because of the electrostatic shielding effect of the brass "holey plate" (see Fig.3) the sweep field was not quite adequate. It is apparent from Fig.'s 2, 10, and 11 that there are present many "old" tracks in addition to the counter tripped ones. This did not present a serious difficulty however, because it was easy to recognize the tracks which were due to particles passing through immediately prior to expansion (i.e., "counter tripped" tracks).

---

* If the camera had been facing in the direction of the gas motion, no distortion would have been observed.

Some evidence of double tracks was noted near the two charged plates. The positive and negative ions are pulled apart by the sweep field before the alcohol vapor condenses on them. Since the sweep field is removed within a millisecond or so, after the counters are tripped, the explanation must be that charges are left on the front glass plate for some time after the sweep potential has been removed. Thus, a residual field remains which may be sufficient to cause separation. Conducting glass would have eliminated this effect, but since only a few of the tracks showed evidence of separation, no effort was made to reduce it.

To illuminate the chamber, argon-filled flash lamps were used. The lamps were 24" long made of 5/16" quartz tubing with tungsten electrodes. A brass semi-cylinder covered the back half of each light over its entire length. When this cylinder was "tickled" with a high voltage pulse, an 80 μf condenser charged to 5,000 volts (2,000 joules) was discharged through the lights. They were filled with 20 cm. of argon after first being outgassed by allowing them to fire several times and re-evacuating. The lights were found to be quite satisfactory, giving sufficient light intensity to allow the tracks to be photographed with an F 11 stop opening in conjunction with the high speed Eastman Recording Negative. The light from these lamps was made into a roughly parallel beam by five - F 1 lenses, $4\frac{1}{2}$ inches in diameter. Because of the finite diameter of the lights, and due to the distortion of the beam, caused by the row of circular lenses (instead of one cylindrical) the beam was, to a certain extent, divergent. The chamber is 3" deep, but

by masking off 1", light was prevented from striking the velvet in spite of this beam divergence.

The cloud chamber was expanded only after two counters were tripped in coincidence by an incoming particle. The counters were argon-petroleum-ether filled, constructed by Professor H. V. Neher. They were placed 22" apart, the lowest 2" above the top of the chamber and the highest 24" (see Fig. 4). Above these was placed a pile of lead blocks 12" high, 24" long and 2½" wide (sufficient to cover the solid angle subtended by the counters). The counters were 10" long and 1 1/8" in diameter giving a coincidence rate of about 2 per minute. Their construction details and operating characteristics can be found in Ref. 2. A schematic diagram of the arrangement of counters, lead and cloud chamber appears in Fig. 4.

III. ELECTRONIC EQUIPMENT

It became apparent very early that in order to make the cloud chamber expand from Geiger counter coincidences, reliable electronic circuits were needed. Following is an outline of the "duty cycle" for a single photograph:

1. The cosmic ray particle passes through both G M counters and then the cloud chamber, producing ion trails in all of them.

2. Because of the multiplicative action of the counters a large number of electrons are initially deposited at the anodes of the counters in a fraction of a microsecond.(3)

3. The negative voltage pulses thus produced are then made

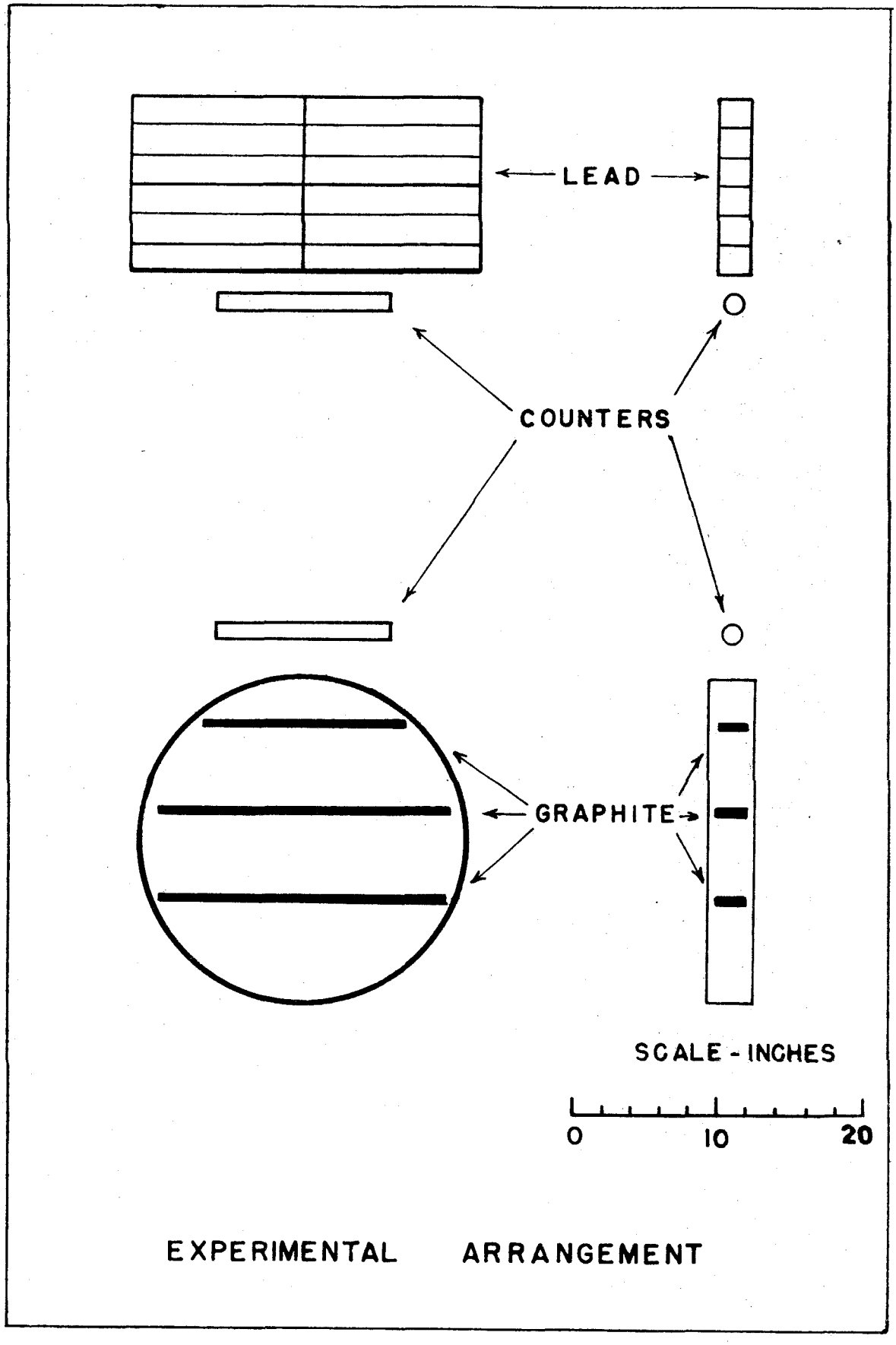

EXPERIMENTAL ARRANGEMENT

FIG. 4

to operate quench circuits which extinguish the counters and simultaneously these pulses are fed into the coincidence circuit.

4. The coincidence circuit gives a pulse only when both pulses are fed into it within a time less than twice the duration of one pulse. The resultant pulse from the coincidence circuit is fed into a "pulse lengthener" which increases its duration to 500 microseconds.

5. The lengthened pulse is fed into the sweep circuit, which turns off the sweep field in the chamber, and also to a circuit which would delay the expansion of the chamber, if necessary. This delay was inserted with the idea of later using the chamber for counting droplets in tracks. Delaying the chamber expansion allows the ions caused by a cosmic ray particle to diffuse for a calculated time before the alcohol vapor condenses on them, forming heavy, immobile droplets. The delay was not used for the work described in this thesis.

6. The delayed pulse is fed into a "light delay" and also to the thyratron (FG 57) which operates the expansion valve for the chamber. The FG 57 is, at the same time, made to operate a relay which starts the recycling motor.

7. The light delay circuit delayed the pulse about 150 milliseconds, allowing ample time for the droplets to grow around the ions formed in 1. The delayed pulse is then put on the grid of an FG 57 which allows .005 coulombs (8.0 μf at 600 volts) to discharge through the primary of a neon sign transformer. The secondary of the transformer is connected to the tickler for the lights. At this point it is appropriate to say

that the shutters of the cameras were left open at all times, since the entire chamber, the light system and the camera system are enclosed in a light-tight cabin (see Section II). Duration of the light pulse has been measured for similar lights and is of the order of 100 micro-seconds.

8. The recycling mechanism turns off the firing circuits (i.e., thyratrons for lights and chamber), turns the cameras one frame, operates a mechanical counter, opens and closes a slow expansion valve and finally shuts itself off. One slow expansion was made after each fast expansion to allow very large droplets to grow on the stray droplet nucleii left in the chamber. These were allowed to fall for about 15 seconds which was sufficiently long to completely clear the chamber.

9. It was found necessary to prevent the light and chamber circuits from being fired for a period of two or three minutes while the cloud chamber returned to thermal equilibrium. To do this a long time delay was devised which made use of the grid-to-plate capacitance of a vacuum tube. A two μf condenser was connected between grid and plate of a 6J5 (amplification factor about 20). Since the equivalent capacity of this circuit is the gain of the tube times the grid-to-plate capacitance the two μf was equivalent to 40 μf. With a 10 Megohm resistor a time constant of 400 seconds was achieved. This circuit, after a given time (which was adjustable) then turned on the thyratron circuits and the apparatus was ready for the next picture.

A block diagram of the principal portions of the electronic

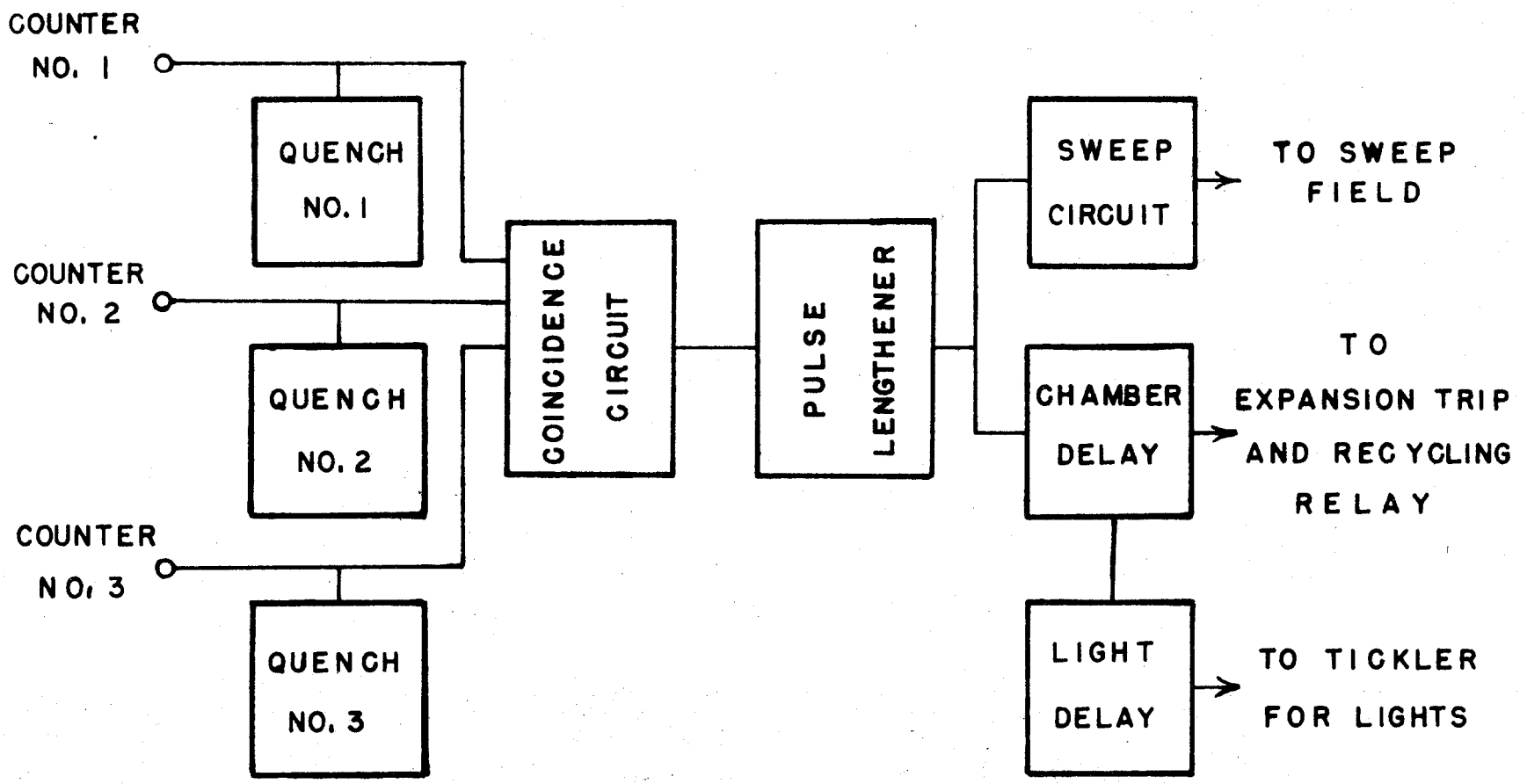

FIG. 5

BLOCK DIAGRAM OF ELECTRONIC EQUIPMENT

equipment appears in Fig 5.

The circuits which performed these various operations were developed by Mr. E. W. Cowan* and myself during the summer of 1946. It was felt that because in the past 4 or 5 years numerous advances in electronic circuit design had been made, it would be appropriate to abandon the conventional Neher-Harper quench circuit, Rossi coincidence circuit, etc. and design some more-or-less original ones.

1. The Quench circuit (fig 6). This is essentially a multivibrator circuit with one tube biased to cut-off. The negative pulse from the counter is capacitatively coupled to the "on" tube. This tube is then cut-off and the other is turned on, the plate dropping 225 volts in the time required to discharge the 500 μf coupling condenser through the tube. Since the plate resistance of a 6SN7 is less than 10,000 ohms, this time is much less than 1 microsecond (C = 10 micro-micro farads app.). The plate voltage drop extinguishes the counter. From the circuit constants (R = 1 Meg. C = 500 micro-micro farads) it is clear that the counter remains extinguished for about 500 micro-seconds. It takes about a 25 volt pulse to operate the circuit, a 200 volt flat-top pulse with a very short rise time being sent on to the coincidence circuit. The Quench circuit and all other multivibrator circuits used utilize $\frac{1}{4}$ watt neon lamps across part of one of the plate resistors. This indicator lamp was found extremely useful in ascertaining whether the various parts of the electronic equipment were operating properly.

---

* Mr. Cowan and I worked for several months together on this project in 1946 and I am greatly indebted to him for all of his inspirational advice and assistance, especially as regards the above circuits.

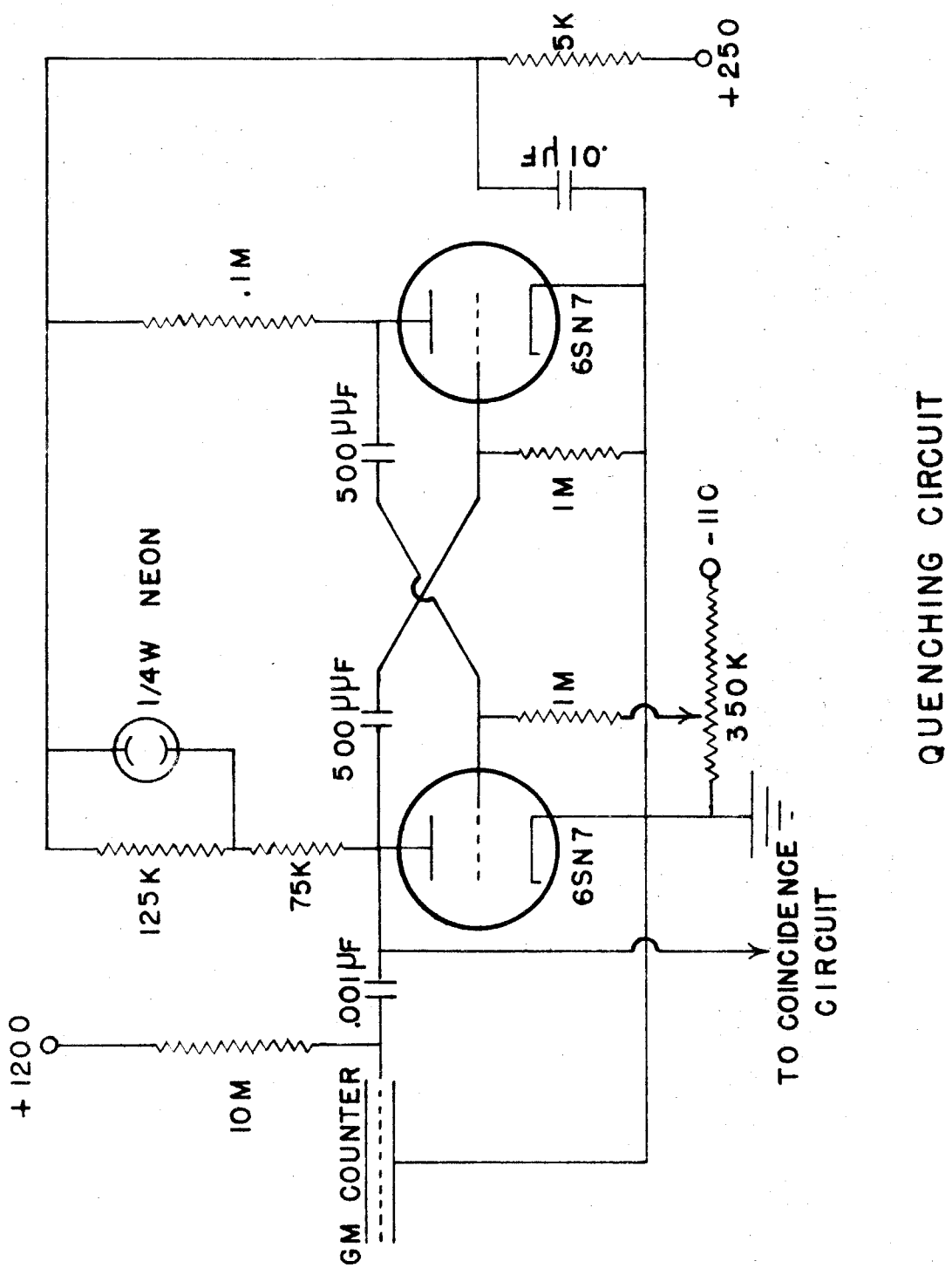
5K
+250
.01 μF
.1M
6SN7
500 μμF
1M
-110
1/4W NEON
500 μμF
1M
350K
125K
75K
6SN7
.001 μF
+1200
10M
GM COUNTER
TO COINCIDENCE CIRCUIT
QUENCHING CIRCUIT

FIG. 6

2. The Coincidence circuit (Fig.7). The leading edge of the square-top pulse was differentiated (R = 20,000, C = 50 micro-micro farads) to a 1 micro-second negative pulse. This was fed into one of three cathode - followers connected with their cathode load resistors in parallel (only two of these were used in our program). Since grid-to-cathode capacitance is negligible for a cathode-follower, the only shunt impedance to the pulse is the 4 micro-micro-farad grid-to-plate capacitance which is small compared with the 50 micro-micro farad coupling condenser. Also the output impedance is small. It is approximately the reciprocal of the transconductance or about 300 ohms. Since the output is fed into a cathode follower inverter stage, the pulse remains essentially undistorted on passing through the coincidence circuit. The operation of the circuit is as follows: If a single pulse is fed in, the cathode voltage drops but little since the other tube effectively shunts the 10,000 ohm cathode resistor. Thus, even though the tube is cut off, if it originally carried 5 milliamperes, the cathode voltage would only drop 1.5 volt (when the other tube is not pulsed its A.C. impedance looking into the cathode is about 300 ohms). However, if the other tube is cut off simultaneously a voltage drop of 10,000 x .010 or 100 volts will occur. The grids are biased positively to give approximately these values. Because of the fast operation of the circuit the two "coincident" pulses must be within 2 microseconds of each other to give a pulse larger than 1.5 volts since the resolving

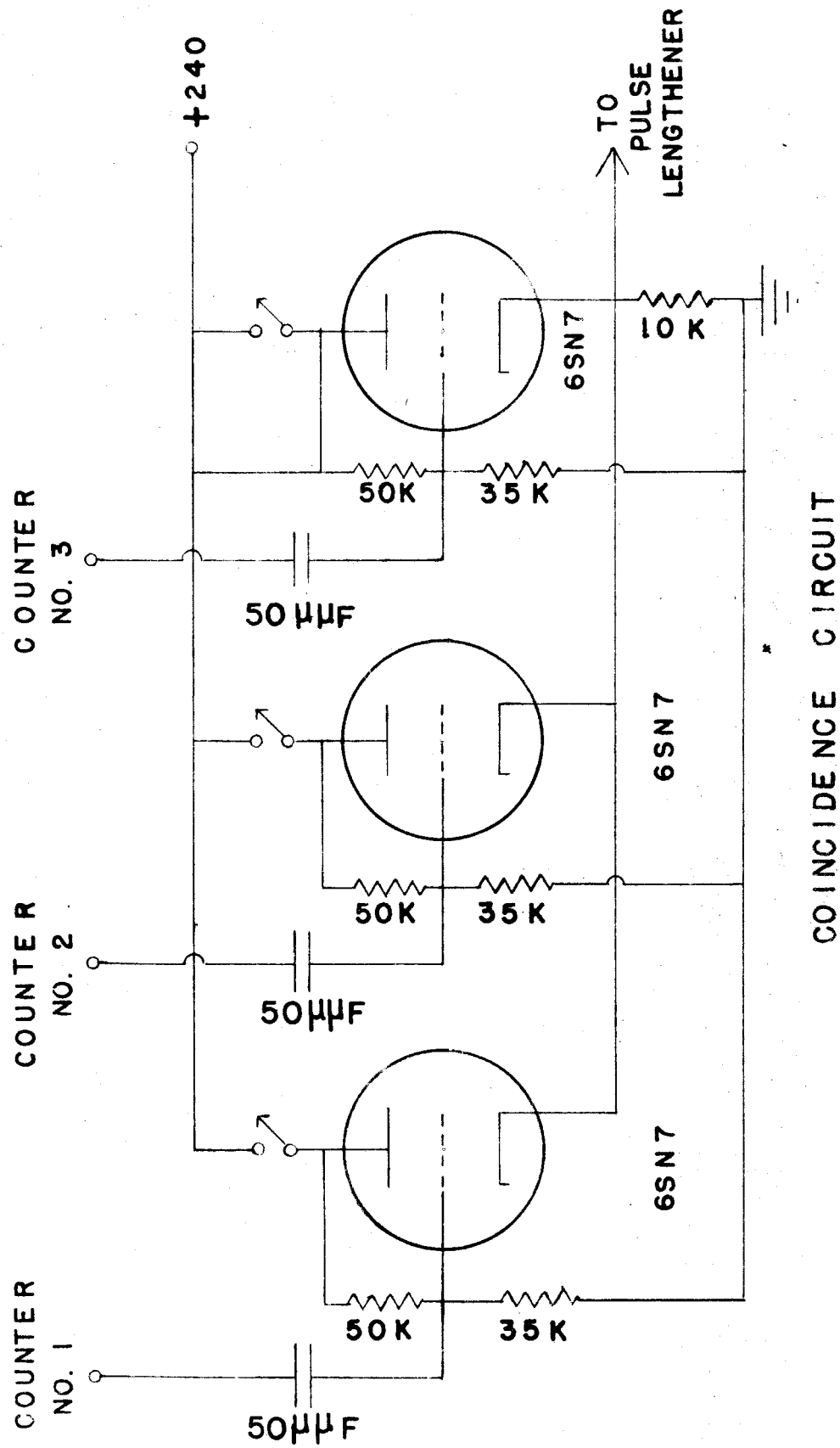
+240
TO PULSE LENGTHENER
6SN7
10 K
50K
35 K
COUNTER NO. 3
50 μμF
6SN7
50K
35 K
COUNTER NO. 2
50μμF
6SN7
50K
35K
COUNTER NO. 1
50μμF
COINCIDENCE CIRCUIT

FIG. 7

time depends only on the differentiating circuit. Although the power supply is well regulated for low frequency changes in load, it was thought advisable to decouple the quench circuit from the rest of the circuits by a 5,000 ohm .01 micro farad RC decoupler, to prevent high frequency "cross talk" between quench circuits and coincidence circuit. Switches were provided with each of the tubes in the coincidence circuit so that 1, 2, or 3 counters could be made to operate in coincidence.

3. The pulse-lengthener (Fig. 8) In order to operate the other circuits without loss in size, the pulse was first inverted to a positive pulse, then fed into a cathode-follower pulse-lengthener. The grid is biased to cut-off, so that when the grid swings positive the cathode follows it, even with the 500 micro-micro farad condenser connected to it, because of the tube's low impedance. However, when the grid swings negative, the cathode no longer follows since the tube is then cut-off. Thus, the pulse is lengthened according to the RC of the cathode impedance, i.e., about 500 micro-seconds. This pulse is again amplified to about 100 volts and simultaneously made to operate a small-loud speaker for audible perception of coincidences.

The delay circuits for lights and chamber, and also the sweep circuit, are very similar in design to the quench circuit except that longer time constants are involved. The sweep circuit removes the 270 volts sweep field for 1 second. The chamber delay is made variable from .01 to 1 second and the light delay from .02 to .2 seconds.

Assuming a 2 micro-second interval over which the coincidence

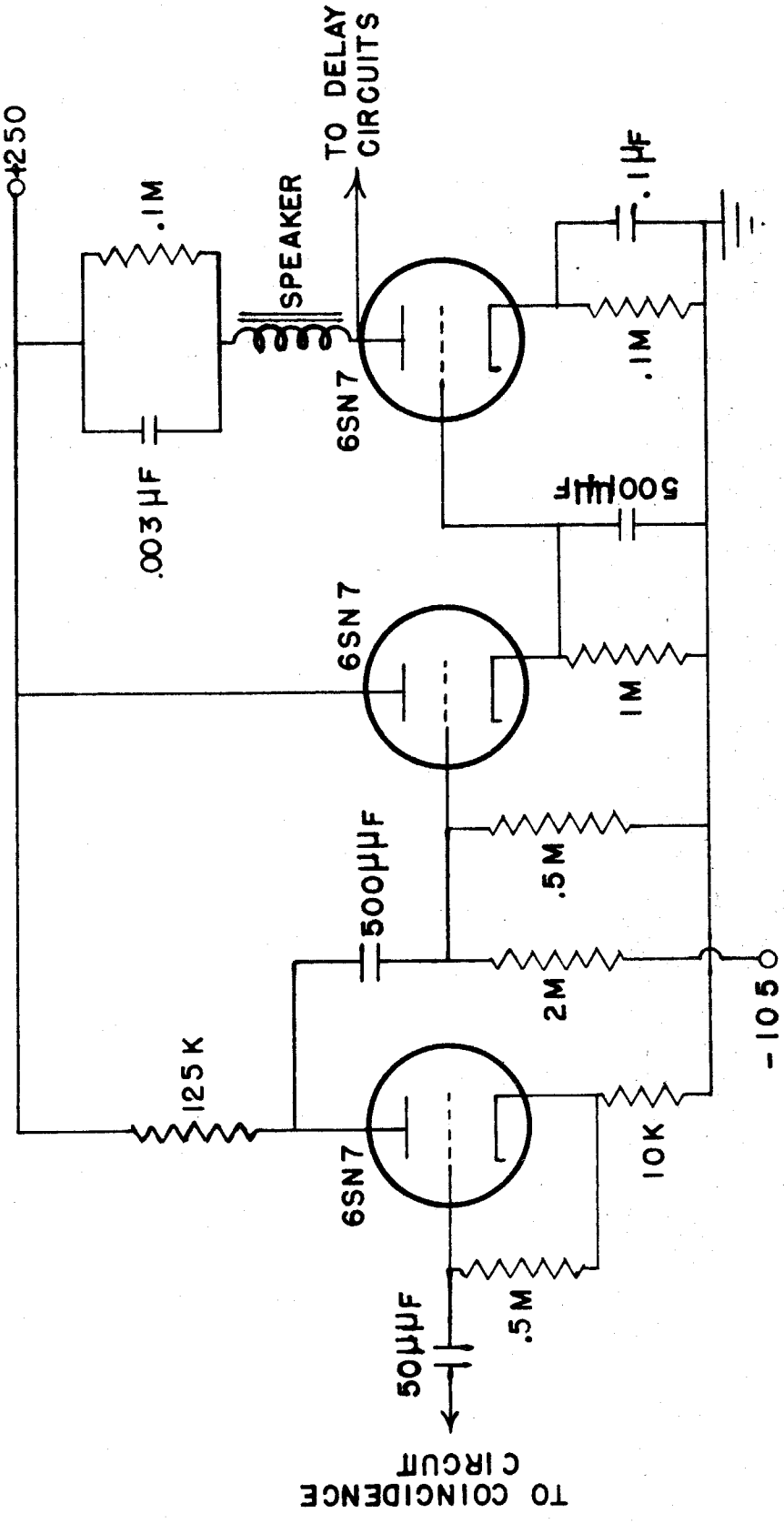
PULSE LENGTHENER
+250
.1M
SPEAKER
TO DELAY CIRCUITS
.1μF
.1M
6SN7
.003μF
500μμF
6SN7
1M
500μμF
.5M
2M
-105
125K
6SN7
10K
50μμF
.5M
TO COINCIDENCE CIRCUIT

FIG. 8

circuit would fire from accidents we can compute the accidental rate:

$N_a = \tau N_1 N_2 =$ # accidentals/sec.

$N_1 = N_2 = \gamma A \Omega$

but $N_c = \gamma A \Omega_c =$ # coincidences/sec

$\Omega_c = A/r^2$ approximately

$\therefore N_a = \tau \gamma^2 A^2 (2\pi)^2 = \tau \left(\frac{N_c}{\Omega_c}\right)(2\pi)^2 =$ 1/120/minute

Ω = solid angle (2π) subtended by one counter

Ω_c = solid angle subtended by 2 counters in coincidence

A = area of counters

γ = # particles/solid angle/ cm.^{2}.

τ = sum of pulse lengths of two counters.

This is less than 1/240 of the coincidence rate.

IV. MEASUREMENT OF TRACKS A single Wilson cloud chamber photograph of the path of a charged particle in a magnetic field enables one to determine the component of momentum of the particle only in the plane of the cloud chamber. This is given by the well-known formula:

$$H\rho = P/ec = \frac{10000}{3} P$$

provided the momentum P is expressed in Mev. the radius of curvature ρ in cm. and the field H in gauss (or oersteds). This component represents very nearly the total momentum for the normal case, ie., where the

particle passing through the chamber trips GM counters above and below the chamber. However, in the case of random tracks, or especially, in the case of knock-on electrons, the other component, i.e., perpendicular to the plane of the chamber may be quite appreciable. With stereoscopic views of the track it is possible to determine this other component quite accurately.

It was mentioned, above, that in our case, the camera axes were inclined at an angle of about 45° with the cloud chamber axis. As a result, if one examines the photographs, one does not observe circles, or even ellipses since the magnification of the camera lens is not constant for all parts of the picture. In fact, to calculate the actual curve on the photograph one must consider the mapping of a constant pitch helix into a 45° plane, where elemental lengths of the helix are magnified according to their distance from the lens. This would give a very complicated relation and it would be hopeless to calculate momenta from it. The path can be determined much easier by reprojecting the pictures. The method by which this was done in our case was as follows:

Both cameras, with the accompanying mirror systems, were lifted as a unit from the gap between the pole pieces and set on a table in front of a large piece of plate glass of dimensions comparable with those of the front glass of the chamber. The backs of the cameras were removed and the negatives were illuminated by a projection lamp and condenser lens system. With the use of the reversibility principle in optics, (this assumes perfect focussing) one can show that the two images of a

point originally in the cloud chamber when re-projected will coincide at a corresponding point in space. If one were to move a ground glass screen back and forth until he found the place where the two images coincided he would then know the exact coordinates of the point with respect to the optical system. This is, in essence, what was done. A large piece of translucent tracing paper was placed over the plate glass. The glass was mounted vertically with face parallel to the mirror system and in such a manner that it could be moved in a direction perpendicular to its face, but not parallel to it. When both images of a track were projected onto the tracing paper, in general one would see two separate tracks intersecting at some point. Moving the glass back and forth would move this point along the tracks. By making a pencil mark on the paper at several of these points (generally 10 - 20 marks per track) and recording opposite each mark the distance that the glass was moved from some fixed point, one had a three-dimensional representation of the track. This could have been done with a great deal more accuracy by using a travelling microscope to record X and Y coordinates (in the plane of the chamber) and the Z coordinate obtained as above. However, our method was somewhat more expedient in view of the large number of tracks measured. The total momentum is easily obtained from these data, viz:

$$H\rho = \tfrac{1}{3} \times 10^4 P$$

$$P_s = \frac{m v_s}{\sqrt{1-\beta^2}}$$

$$P_z = \frac{m v_z}{\sqrt{1-\beta^2}}$$

where:

P_s = Component of momentum in plane of the chamber.

P_z = Component along axis of chamber.

$$\beta^2 = \frac{v_z^2 + v_s^2}{c^2}$$

$$v_s^2 = v_x + v_y^2$$

Therefore, the momenta are proportioned to the velocities which in turn are proportional to the distance travelled in their respective directions in the same length of time. Hence, by plotting distance along the measured circle against distance the glass plate was moved, as given by the numbers opposite each point, one obtained from the mean slope of this curve the ratio of momenta,

viz:

$$\frac{P_z}{P_s} = \frac{dz}{ds} = \text{slope of curve}$$

$$P^2 = P_s^2 + P_z^2$$

$$P = P_s \sqrt{1 + \left(\frac{dz}{ds}\right)^2}$$

V. ACCURACY OF DATA In general the tracks were very nice circles when reprojected and plotted in this manner, most radii being measurable to 3 per cent or better. However, the slopes were much less accurate, being occasionally uncertain by 30%. The maximum value of $\frac{dz}{ds}$ recorded in our data was 1.2, but most values were less than 0.3. This made the error in momentum, in general, less than that due to radii measurement. Thus, although there was considerable distortion due to motion of gas along the cloud chamber axis, this rarely caused much error in the momentum determination. However, in several instances, especially for the low

energy knock-ons where the angle of emergence from the plate is often quite large, considerable errors were introduced.

Some of the errors in curvature measurement are undoubtedly due to the method of plotting. After the pencil marks were placed on the tracing paper, circles were fitted to them. Because of the finite size of the marks and because of errors in estimating the intersection of the tracks the deviation of each mark from the circle did not always vary in a uniform manner (as would be produced by distortion) but were more or less random. This, I believe, caused at least half of the 3% error mentioned above. Use of a travelling microscope arrangement may have eliminated this.

Another possible source of error, especially in the energy loss data, is inhomogeneity in the magnetic field. A plot of the field intensity as a function of vertical distance from the center of the chamber appears in Fig. 9. The variation is similar for horizontal distances. It is seen that although the field drops off very rapidly at the edge of the pole face, it is uniform to within 5% of the value at the center over the region occupied by the cloud chamber ($\pm$ 2½% of mean value). There is in addition to this a 2% variation along the axis which is not plotted. The value of the field chosen for the calculations below was the value at the center, since most of the events recorded occurred somewhere near this. Its absolute value is believed to be accurate to $\pm$ 2%. The field varied considerably during a day's run due to heating of the copper coils of the magnet. This

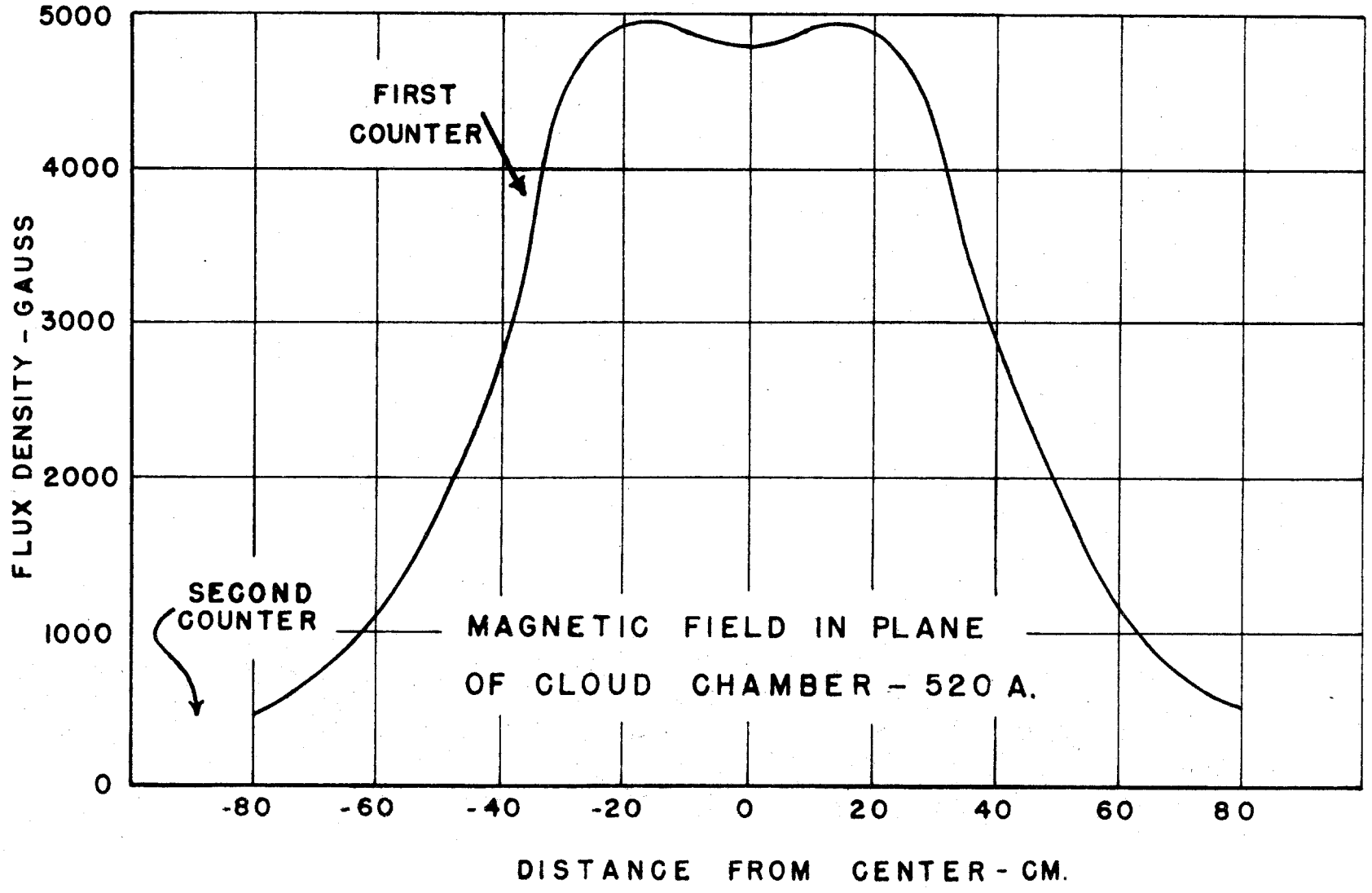
5000
4000
3000
2000
1000
0
FLUX DENSITY - GAUSS
FIRST COUNTER
SECOND COUNTER
MAGNETIC FIELD IN PLANE OF CLOUD CHAMBER - 520 A.
-80
-60
-40
-20
0
20
40
60
80
DISTANCE FROM CENTER - CM.

FIG. 9

necessitated frequent anmeter readings, but it is believed that the value of the magnetic field chosen for each picture is well within the over-all probable error.

VI. THEORY OF ENERGY LOSS When high energy charged particles pass through matter they lose energy in any of several ways. These may be divided into two distinct types:

1. Energy loss by collision, i.e., by interaction with the orbital electrons of the atoms in the material traversed.

2. Energy loss by radiation, i.e., rapid decelerations of the charged particle upon collision with a nucleus, cause the particle particle to radiate a photon.

The theory of each of these processes will be discussed briefly.

1. Collision Loss. The theory of collision loss was first investigated by Bohr[4] using a classical picture. It was later given a quantum-mechanical treatment by several investigators,[5, 6, 7, & 8] the latest of which was by Bhabha in 1938[8] This type of energy loss may also be divided into two groups according to the method of theoretical treatment. The first, "Energy loss by excitation and ionization" results from the momentum imparted to the electrons in the atom when a fast moving charged particle passes by at a distance great enough so that the direction of motion of the moving particle is not changed appreciably. Bethe[6] has given for the energy loss per centimeter:

$$\left(\frac{dE}{dx}\right)_1 = \frac{2\pi n_e r_0^2 \mu_e}{\beta^2}\left[\log \frac{2\mu_e \beta^2 \eta}{(1-\beta^2) I^2 Z^2} - \beta^2\right]$$

For energy losses which are not greater than η per collision. In this equation, n_e is the number of electrons per cm.^{3}, r_0 is the classical electron radius, μ_e is the rest energy of the electron, β is the ratio of the velocity to that of light, and IZ is the "average ionization" of the matter traversed, I being a numerical constant equal to about 13.6ev. Bethe's formula also contains two terms involving Euler's ψ function, but these terms can be neglected provided $\beta >> \frac{1}{137}$. The formula is valid for any kind of charged particles under the approximation mentioned.

The second type of collision loss, "Loss by close collision", arises from strong interaction between the moving particle and the electrons, resulting in the electrons being ejected from their orbit with a large fraction of the energy of the moving particle. The secondary electron so obtained is frequently spoken of in the literature as the "knock-on electron". The early method of treatment[4] was to consider, in the center of mass system, the Rutherford scattering of the electron from the fast particle. Quantum-Mechanical treatments considers, in addition, the spin interactions between the two particles and also the quantum mechanical exchange forces. The formulae given for the probability of ejecting a secondary of energy between q and q + dq by a primary of energy E, in a distance dx, for 3 kinds of particles is:

1. Electron[5]

$$\chi(E,q)\,dq\,dx = 2\pi n_e r_0^2 \mu_e \frac{dq\,dx}{\beta^2}\left[\frac{E}{q(E-q)} - \frac{1}{E}\right]^2$$

2. Positron[8]

$$\chi(E,q)\,dq\,dx = 2\pi n_e r_0^2 \mu_e \frac{dq\,dx}{\beta^2 q^2}\left[1 - \frac{2q}{E} + 3\left(\frac{q}{E}\right)^2 - 2\left(\frac{q}{E}\right)^3 + \left(\frac{q}{E}\right)^4\right]$$

3. Mesotron of spin 0[8]

$$\chi(E,q)\,dq\,dx = 2\pi n_e r_0^2 \mu_e \frac{dq\,dx}{\beta^2 q^2}\left(1 - \beta^2 \frac{q}{q_m}\right)$$

where q_m is the maximum energy transferred to the electron. We note that if $q \ll E$ all three formula's reduce to:

$$\chi(E,q)\,dq\,dx = 2\pi n_e r_0^2 \mu_e \frac{dq\,dx}{\beta^2 q^2} \;*$$

which is the classical formula given by Bohr.

Integrating this expression we get:

$$\left(\frac{dE}{dx}\right)_2 = \int_\eta^{q_m} q\,\chi(q)\,dq = 2\pi n_e r_0^2 \frac{\mu_e}{\beta^2} \log \frac{q_m}{\eta}$$

---

* It is significant that this formula does not contain the primary energy, E, if $\beta \sim 1$.

Adding the two expressions for energy loss we obtain for the total collision loss per centimeter for collisions with not too large an energy loss: i.e., $E >> q$

$$\frac{dE}{dx} = \frac{2\pi n_e r_o^2 \mu_e}{\beta^2}\left[\log\frac{2q_m\mu_e\beta^2}{(1-\beta^2)I^2Z^2} - \beta^2\right]^*$$

For a heavy particle: $q_m = \dfrac{E^2 - M^2c^4}{Mc^2\left(\frac{m}{2M}+\frac{M}{2m}+\frac{E}{Mc^2}\right)}$ while, for an electron, we get only half this (i.e., $E/2$) for the reason that if the secondary electron had energy greater than this it would be mistaken for the primary, since in the case of the electron the two are indistinguishable.(9) It can be seen that for $\beta \sim 1$, since the logarithm changes very slowly, the energy loss is more-or-less constant, independent of primary energy.

The range of the particle can be found from the energy-loss curves by direct integration:

$$R = \int_0^{km} dx = \int_E^0 \frac{dE}{(dE/dx)} \simeq \frac{E}{\left(\frac{dE}{dx}\right)_{AV.}}$$

---

* Integration of the exact collision cross-section for electrons gives:

$$\frac{dE}{dx} = \frac{2\pi n_e r_o^2 \mu_e}{\beta^2}\left[\log\frac{2\mu_e\beta^2 q_m}{(1-\beta^2)I^2Z^2} + 1-\beta^2 - \left\{2-\left(1-\sqrt{1-\beta^2}\right)\right\}^2 + \tfrac{1}{8}\left(1-\sqrt{1-\beta^2}\right)^2\right]$$

2. Radiation Loss The theory of radiation loss of electrons has been worked out in detail by Heitler.[10] The results obtained are in a form which is rather involved for purposes of computation. An approximate formula is:[10]

$$\frac{dE}{dx} = 4\alpha N Z^2 r_0^2 E \log \frac{2E}{\mu_e}$$

provided $\mu_e << E << 137 \mu_e Z^{-1/3}$

or $$\frac{dE}{dx} = 4\alpha N Z^2 r_0^2 E \left[\log(183 Z^{-1/3}) + 1/18\right]$$

if $137 \mu_e Z^{-1/3} << E$

where α is the fine structure constant and N is the number of atoms per cm^3. Since the logarithm is roughly constant for both cases it is seen that both formulae give an energy loss roughly proportional to the energy.

Considering both types of losses together, a rough idea of the relative importance of the two can be obtained in the region near the minimum in the collision loss curve:

$$\frac{\left(\frac{dE}{dx}\right)_{rad.}}{\left(\frac{dE}{dx}\right)_{coll.}} \approx \frac{ZE}{700} \qquad \text{for electrons}$$

(8)

For heavy particles this ratio becomes:

$$\frac{\left(\frac{dE}{dx}\right)_{rad.}}{\left(\frac{dE}{dx}\right)_{coll.}} \approx \frac{ZE}{700}\left(\frac{m}{M}\right)^2$$

Thus for electrons of low energy and for nearly all heavy particles, radiation loss in carbon ($Z = 6$) is negligible.

VII. SUMMARY OF PREVIOUS RESULTS. The experimental data of previous investigators with regard to collision loss is rather meager, especially for elements of low atomic number. Some of the earliest work was done by Anderson and Neddermeyer.(11) They reported that for five cases of energy loss in a 1.5 cm. carbon plate with initial energies between 12 and 34 Mev., the average loss was about 5 Mev. per cm. They also presented some knock-on data. For 587 traversals of the 1.5 cm. carbon plate, 26 secondaries were observed with energies lying between 1 and 100 Mev. This agrees with the theoretical formula (above) within the experimental error.

Turin and Crane,(12) using the β rays from Li^8 which lay in an energy range of 4-6 Mev., obtained an average energy loss of 1.70 Mev. in $\frac{1}{2}$ cm. of carbon which is in very good agreement with that predicted by theory for this energy range.

VIII. EXPERIMENTAL RESULTS

1. Energy Loss In our cloud chamber we observed 38 traversals of the graphite plates for which the momenta before and after entering the plate could be determined with a fair degree of accuracy. The incident energies involved ranged from 3 to 25 Mev. In eight cases a single particle made more than 1 traversal. (Fig. 10 shows a particle losing a measurable energy in each of five traversals and stopping on the sixth). In all these cases it was possible to measure the energy loss to a high degree of accuracy since:

A. A large portion of each circle representing the electron trajectory (in most cases a complete semi-circle) was found within the illuminated region -

B. The tracks were confined within a smaller region of the cloud chamber, hence the magnetic field would be quite homogeneous for all parts of the track. This is, of course, characteristic of all low energy tracks.

All of the data obtained are plotted in Fig. 12. The probable errors indicated represent only the limits of accuracy set by measurement of the tracks (which neglects inhomegenety in the field) but this is believed to be the major part of the experimental error. The theoretical curves for collision and radiation loss are plotted on the same graph.

It is at once evident from the graph that the deviation of individual points from the theoretical is, in nearly all cases, much greater than the probable error. Also it is fairly clear that the deviations are

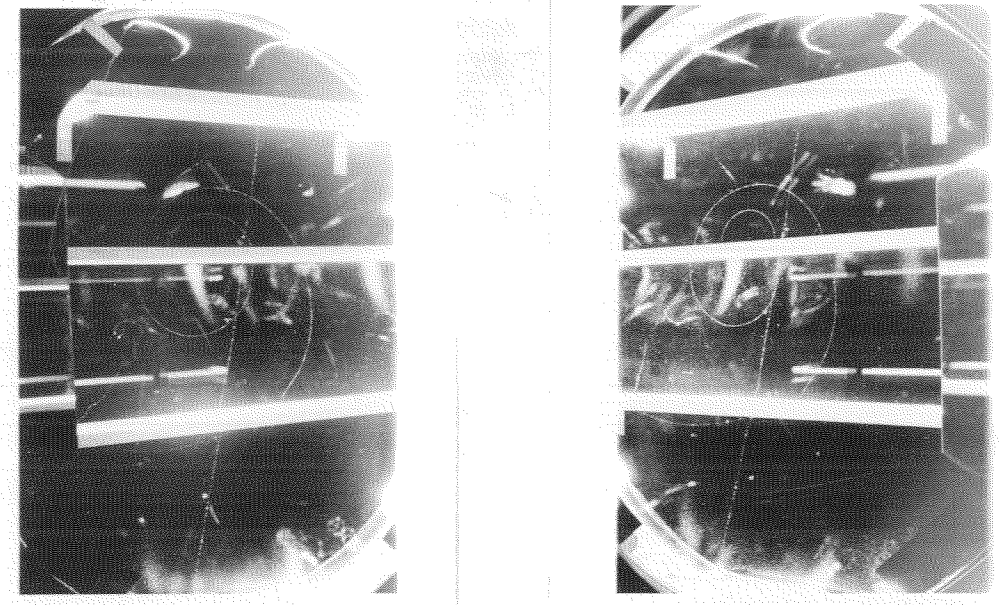

FIG. 10

An electron of 28 Mev. energy loses a measurable amount of energy in each of five traversals and stops on the sixth. A highly scattered (or distorted) track can be seen entering the lower plate at the left just above the origin of the electron track possibly giving rise to it, but probably not related.

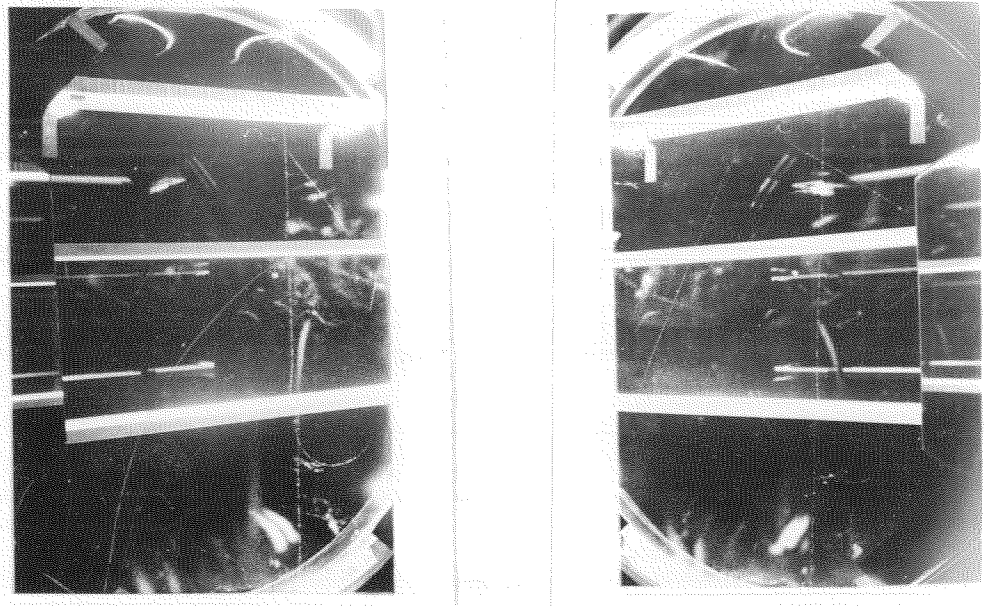

FIG. 11

Typical Knock-on - 6.5 Mev.

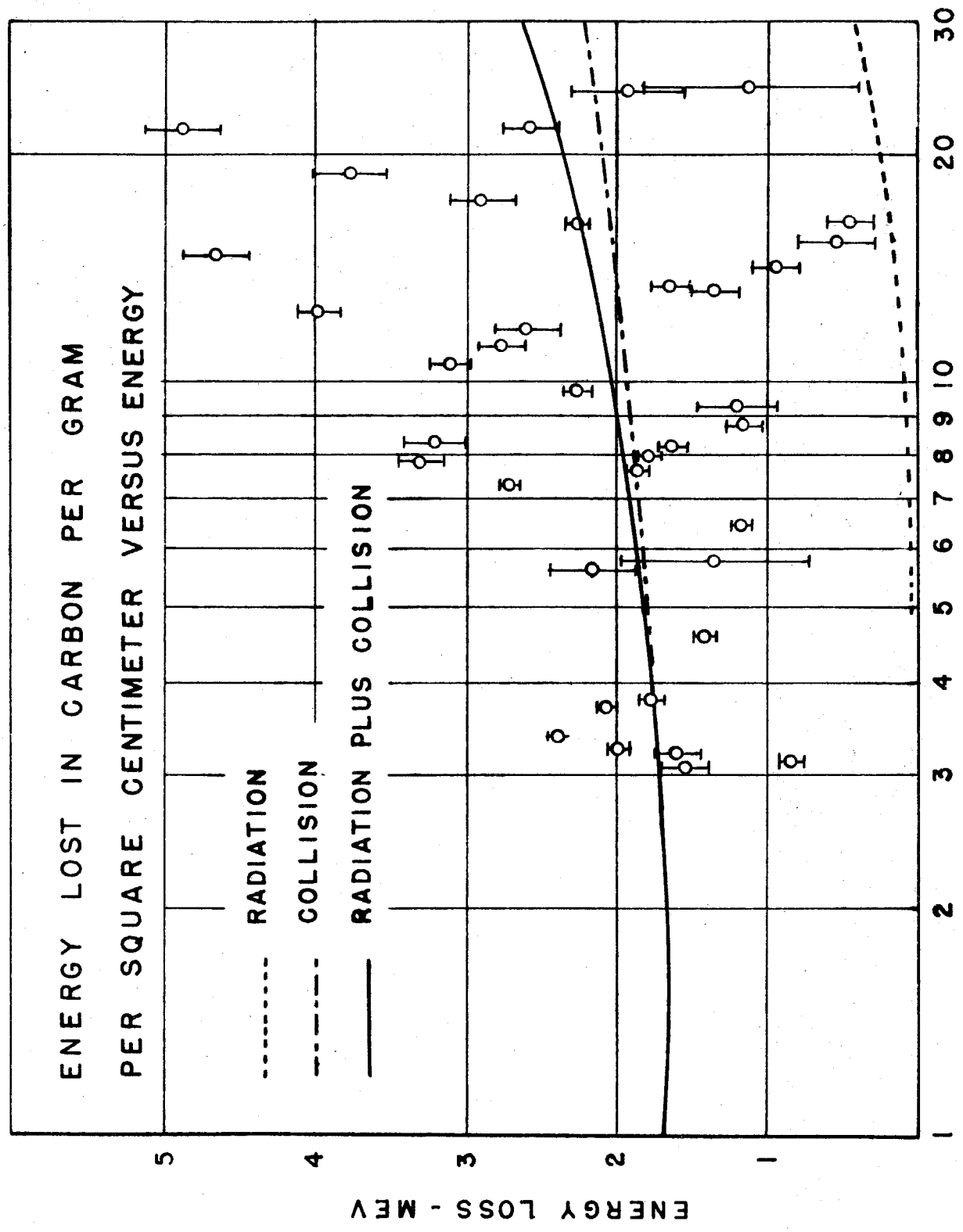
ENERGY LOST IN CARBON PER GRAM
PER SQUARE CENTIMETER VERSUS ENERGY
RADIATION
COLLISION
RADIATION PLUS COLLISION
ENERGY LOSS - MEV
ENERGY - MEV
1
2
3
4
5
10
20
30

FIG. 12

greater, the higher the energy.* These large deviations are inherent in the theories of the two types of energy loss. It must be remembered that the formulas presented in Section VI represent the average energy loss only after traversing a given thickness of matter. This average is the result of a great many interactions with the atoms in the material traversed. Statistically the greater the number of interactions of a given kind, the smaller will be the error in the average value. But if all interactions had the same average lost, say q, the number of interactions with this loss, is proportional to $1/q$, hence, the greater accuracy in the mean is obtained if:

A. Most of the energy losses per interaction are small and-

B. The amount of matter traversed is large.

In the case of collision loss, the probability for an energy loss q is proportional to $1/q^2$, whereas in the case of radiation it is proportional to $1/q$.[13] This, in the case of radiation for a given thickness of plate, q, the mean energy loss in the plate, can result, with equal probability, from only a few large energy transfers as from many small ones. For collision loss, the possibility of large energy transfers is much smaller. An argument of this sort leads to the conclusion that "the straggling due to inelastic collisions will not be very large..... The straggling is, however, characteristic of the energy loss by radiation." (Quotation from Heitler p.224)

---

* Of course, the probable error in measurement also increases with energy since the curvatures are smaller and because the percentage change in curvature is smaller. However, the deviations are still much greater than the probable errors, even at the highest energies measured.

Thus, in our case, at the low energies, where radiation loss is small, the only straggling present is that due to collision. This is still appreciable, but much smaller than at higher energies where losses over twice the theoretical were observed. In fact, one track was observed (Fig. 2) in which an electron of 88 Mev. energy enters the bottom plate from above and one of 36.1 Mev. leaves below. The energy lost is seven times the theoretical sum of collision plus radiation loss, even though the mean radiation loss at this energy is still only half the collision loss.

By dividing the 37 experimental points into four groups of roughly nine in each, the curve was smoothed out considerably (Fig. 13). The probable errors indicated in Fig. 13 are now probable errors of the means. That is, they were computed from the formula:

$$\text{P. E.} = \frac{.6745}{n}\sqrt{\sum_{i=1}^{n}(K_i - \bar{K})^2}$$

It is seen that in each case the deviation from the theoretical is within the probable error.

2. Knock-on data From 3,884 traversals by cosmic ray particles of the graphite plates, 164 visible secondaries are ejected, all of them of negative sign.* Since pairs produced by bremsstrahlen from the primaries, or secondaries emitted by nuclear disruptions would give rise

---

* Fig. 13 shows a typical knock-on of 6.5 Mev. energy

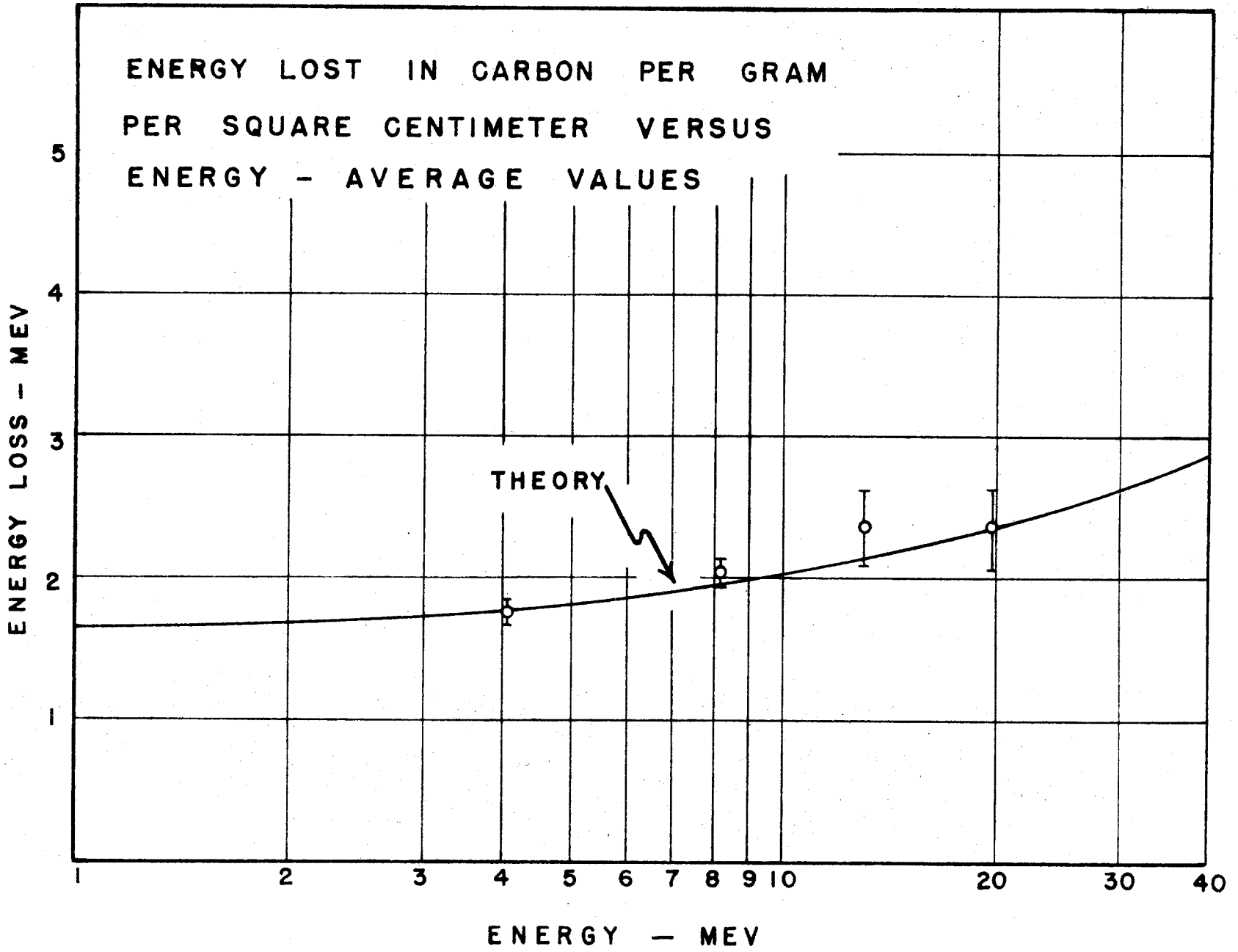
ENERGY LOST IN CARBON PER GRAM
PER SQUARE CENTIMETER VERSUS
ENERGY - AVERAGE VALUES
THEORY
ENERGY LOSS - MEV
ENERGY — MEV
1
2
3
4
5
6
7
8
9
10
20
30
40

FIG. 17

to some positives we conclude that all secondaries observed are knock-on electrons. Out of this number 43 were not used either because of objectionable distortion, because they left the illuminated region too soon to give a reliable curvature measurement or because they were just too faint to measure accurately. Also, eight more were rejected because they were from primaries of 300 Mev. or less. The results of the remaining 113 are tabulated in Table 1 and are plotted in Fig. 14 using overlapping intervals.

To apply the theory of Section VI to our data requires a little calculation. We had, for the probability of producing a secondary of energy between q and q + dq in an element of length of the material, dx, from a primary mesotron of energy E:*

$$\chi(E,q)\,dq\,dx = \frac{K\,dq\,dx}{q^2}\left[\frac{1}{\beta^2} - \frac{q}{q_m}\right]$$

Where: $K = 2\pi n_e r_0^2 N_e$

and $$q_m = \frac{E^2 - M^2c^4}{Mc^2\left(\frac{m}{2M} + \frac{M}{2m} + \frac{E}{Mc^2}\right)}$$

If $M \gg m$ and $E \ll \frac{M}{2m} \cdot Mc^2 = 10$ Bev,

---

* The primaries, in our case, are nearly all mesotrons since the 12" of lead above the cloud chamber filters out the electrons.

TABLE I

Energy Interval (Mev.)	Number of Secondaries	Av. Energy	Number per Mev.	Theoretical
30-70	9.0	50.0	.23	.08
25-55	9.0	40.0	.30	.14
20-30	8.0	25.0	.80	.42
15-25	8.0	20.0	.80	.64
10-20	14.0	15.0	1.40	1.24
8-15	18.0	11.5	2.57	2.15
6-10	14.0	8.0	3.50	4.13
5- 8	18.0	6.5	6.00	5.85
4- 6	20.0	5.0	10.00	9.20
3.5- 5	17.0	4.1	11.35	12.55
3- 4	14.0	3.5	14.00	16.30
2.5-3.5	18.0	3.0	18.00	20.50
2- 3	17.0	2.5	17.00	27.40
1-2.5	8.0	1.6	8.00	56.50
0- 2	7.5	1.0	7.50	--
0- 1	4.0	0.5	4.00	--

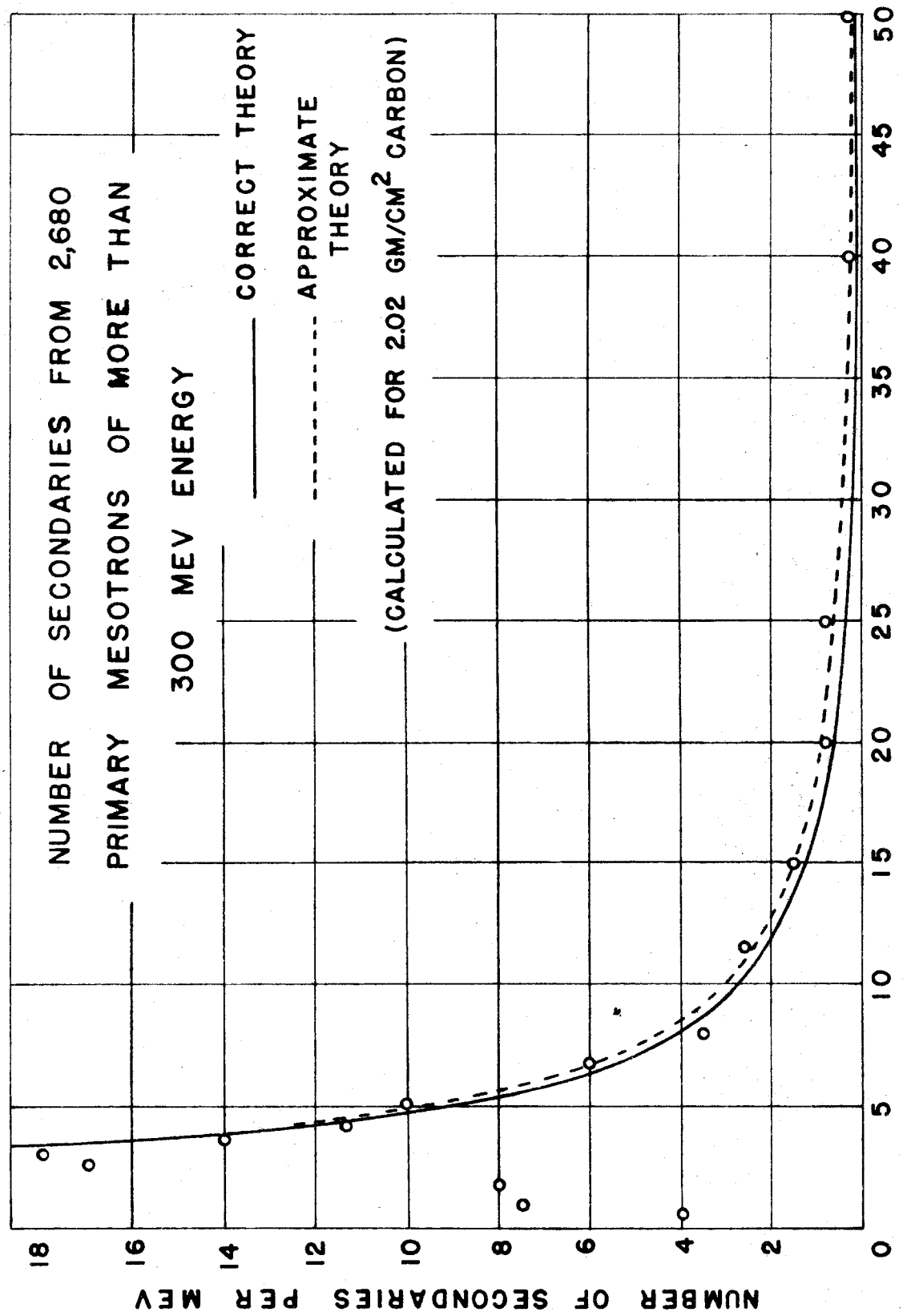
NUMBER OF SECONDARIES FROM 2,680
PRIMARY MESOTRONS OF MORE THAN
300 MEV ENERGY
CORRECT THEORY
APPROXIMATE THEORY
(CALCULATED FOR 2.02 GM/CM^2 CARBON)
NUMBER OF SECONDARIES PER MEV
ENERGY OF SECONDARIES --- MEV
0
2
4
6
8
10
12
14
16
18
5
10
15
20
25
30
35
40
45
50

FIG. 14

q_m can be written:

$$q_m = \frac{2\mu_e \beta^2}{1-\beta^2}$$

Thus, the probability becomes:

$$\chi(E,q)dq\,dx = \frac{K\,dq\,dx}{q^2}\left[\frac{1-\frac{q}{2\mu_e}\left(\frac{Mc^2}{E+Mc^2}\right)^2}{\beta^2}\right]$$

It is seen that for E = 300 Mev. and for q as low as 10 Mev. the second term is $\sim 5/8$ and hence cannot be neglected. This is unfortunate since it involves a knowledge of the primary energy spectrum under the 30 cm. of Lead (+4.0 cm. of steel support). This spectrum has been calculated in the appendix; (Fig. 15) call this distribution function P (E). The probability now becomes

$$\chi(q)dq\,dx = \frac{K\,dq\,dx}{q^2}\int_{E=E_m(q)}^{\infty} P(E)\left\{1-\frac{q}{2\mu_e}\left(\frac{Mc^2}{E+Mc^2}\right)^2\right\}dE$$

Where E_m (q) is the minimum energy that will give a knock-on of the value q, or it is equal to 300 Mev. if this value lies below 300. Since E $\geqslant$ 300 Mev. β^2 can be taken as 1 (with a maximum of 6% error). To save labor in calculation, we have taken E_m (q) = 300 Mev. for <u>all</u> q's. This is exact for q $\leq$ 15 Mev. Thus, to a first approximation,

---

* See footnote on previous page concerning the expression in brackets.

we get:

$$\chi(q)\,dq\,dx = K\left[\frac{dq}{q^2} - G\,\frac{dq}{q}\right]$$

where $\int_{300}^{\infty} P(E)\,dE = 1$

and $G = \int_{300}^{\infty} \frac{P(E)}{2\mu e}\left\{\frac{Mc^2}{E+Mc^2}\right\}^2 dE$

The integral defining G has been evaluated numerically, whence $G = 8.07 \times 10^{-3}$. The knock-ons may be produced at any distance, "x", below the upper surface of the graphite plate. To get the distribution of energies q' below the plate, we integrate the above expression obtaining:

$$P(q') = \int_0^t \chi(q(x))\,dx$$

where: $q'(x) = q(x) - \int_x^t \frac{dq}{dx}\,dx \approx q(x) - 3.6(t-x)$

since $\frac{dE}{dx}\cdot t = 3.6\ \text{MeV/gm./cm}^2$

We thus get:

$$P(q')\,dq' = \frac{K}{3.6}\left[\frac{1}{q'} - \frac{1}{q'+3.6} - G\log\frac{q'+3.6}{q'}\right]dq'$$

since $dq' = dq$

Multiplying P(q') by the number of traversals (in our case $3,884 \times \frac{113}{164} = 2,680$) gives the total number of secondaries expected below the graphite plates. The correction term due to G is small except at the higher energies where the experimental error is large anyway. Both curves are plotted with the data in Fig. 14 (uncorrected curve dotted). It is seen, that except at the very low energies the agreement is fairly good. The drop at the low end is to be expected because:

1. Many more of the low energy knock-ons are missed when viewing the photographs, since they occupy such a small area on the photograph. A 1 Mev. electron has a radius of curvature of only 1 cm. in our chamber.
2. The angle between primary and the low energy secondary is large, hence many of the low energy knock-ons never reach the illuminated region below the plate.
3. Scattering of low energy secondaries is large, hence they lose more energy on the average than the simple theory predicts due to the greater path length in the graphite.

IX. CONCLUSIONS The loss of energy in graphite plates, even though statistical fluctuations are great, seems to agree very well with that predicted by present theories. The range of energy over which this agreement holds has been extended up to 25 Mev. by the work presented in this thesis.

Further extension will be difficult since:

1. The changes in curvature become much smaller at higher energies. Thicker plates would help this.
2. Radiation loss becomes quite large and as a result it is difficult to isolate it from the collision loss.

The knock-on spectrum follows quite well the inverse square law as anticipated by simple theory. It has been postulated from the frequency of burst excitation by mesotrons[14] that the spectrum should follow an inverse first power law. Unfortunately our data does not give any information concerning burst excitation, because the limit of knock-on energies measured is only about 50 Mev. whereas the portion of the spectrum which is responsible for the bursts is at a much higher energy. More data on the high energy spectrum would certainly be desirable for this reason. It would also be quite valuable in determining the spin of the mesotron since, at higher energies, the spectrum is spin dependent.[8]

APPENDIX

The probability of a mesotron stopping in the chamber depends very critically on the sea-level energy spectrum. Anderson and Neddermeyer, Blackett, LePrince-Ringuet, Hughes and Jones[11,15,16, 17, 18] and others have determined this under various conditions. All spectra agree pretty well in form, but differ somewhat in the location of the maximum. The most recent work, by Hughes and Jones, using 660 tracks of particles filtered through 10 cm. of lead is represented in Fig. 15. Although a smooth curve is plotted, it must be kept in mind that fluctuations, especially at the low end of the spectrum are great.

From a knowledge of this energy spectrum and of the range-energy relation for mesotrons in lead, one can calculate the percentage of the mesotrons that stop in the cloud chamber. We wish to know how many mesotrons that pass through "x" gm./cm.^{2} of lead will stop in an additional "dx" gm./cm.^{2} of graphite. We have

$R = R(E)$ = Range of the primary whose energy is E.

$$dR = \frac{\partial R}{\partial E} dE = dx$$

Hence, if we know $\frac{\partial R}{\partial E}$ we get dE and from this we find, using the energy spectrum, the fraction of mesotrons lying in the interval dE. But $\frac{\partial R}{\partial E} = \left(\frac{dE}{dx}\right)^{-1}$ which is just the value given by the formula in Section VI (taken at the energy corresponding to "x"). In our case x = 260 gm./cm.^{2}. (Although the amount we actually used was 374 gm./cm.^{2}

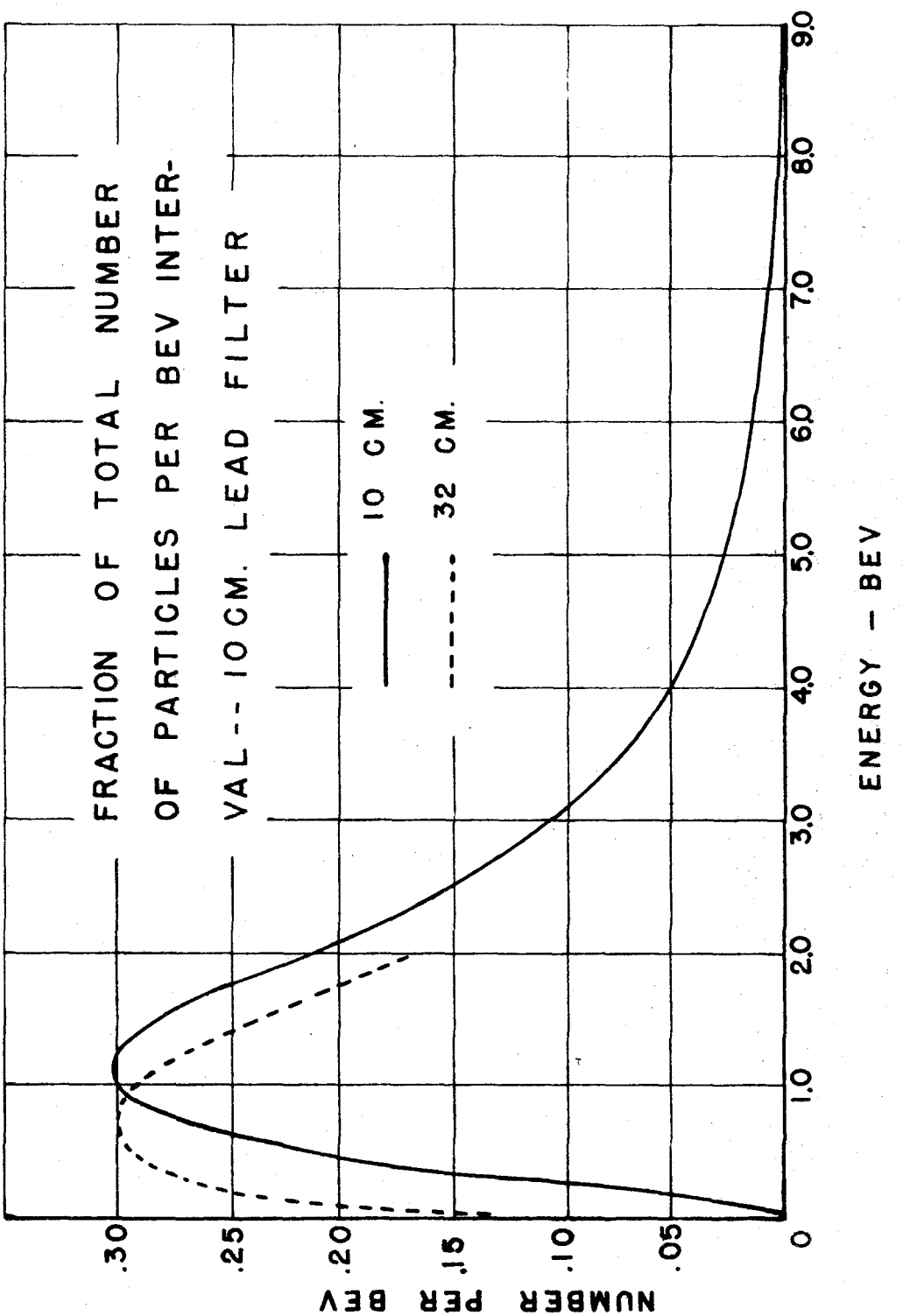
FRACTION OF TOTAL NUMBER
OF PARTICLES PER BEV INTER-
VAL -- 10 CM. LEAD FILTER
10 CM.
32 CM.
NUMBER PER BEV
.30
.25
.20
.15
.10
.05
0
1.0
2.0
3.0
4.0
5.0
6.0
7.0
8.0
9.0
ENERGY - BEV

FIG. 15

Hughes' curve is under 114 gm./cm.^{2}.) Therefore, pc = 445 Mev. From the graph in Fig 15, we find that at this momentum, .018% of all particles lie in a 1 Mev. range. Thus, for the 2 gm./cm.^{2} (1.1 cm. graphite plate) used in the chamber we get:

$$dN = 1.8 \times 10^{-4} \times 2 \times 2.0 = .72 \times 10^{-3}$$

That is, one out of every 1,400 particles which traverse any of the graphite plates should stop.

In a similar manner one can actually calculate the energy spectrum below the lead plate. If we denote the number of mesotrons above the plate of energy between E_0 and $E_0 + dE_0$ by N_0 and below the plate of energy E by N, we have:

$$N(E)\,dE = N(E_0)\,dE_0$$

$$\text{or } N = N_0 \frac{dE}{dE_0}$$

$$\therefore N = N_0 \left(\frac{dE_0}{dx}\right) \Big/ \left(\frac{dE}{dx}\right)$$

where $\frac{dE_0}{dx}$ is the rate of energy lost at the energy E_0 (roughly constant) and $\frac{dE}{dx}$ at the energy E. For large E, $\frac{dE}{dx}$ is also roughly constant and equal to $\frac{dE_0}{dx}$ hence, the shape of the curve is unchanged, but the whole curve is moved to the left, a distance determined by the mass of lead

used (in our case the distance moved is 300 Mev.). This places the peak in the energy spectrum down in the low energy region in which we are interested. The actual spectrum obtained is plotted in Fig. 15 and the low energy end of the spectrum replotted in Fig. 16.

Now a 17.5 Mev. mesotron of mass 200 will stop in 2 gm./cm.^{2} of graphite. Thus, integrating the curve from zero to 17.5 Mev. gives the total number stopping in a 1.1 cm. graphite plate. A rough numerical integration gave $\frac{1}{1,300}$ stopping (checking the above value, of course). However, this curve gives some additional information about the percentage of particles that should stop which lie in the very low energy region. Although the magnetic field (Fig. 9) drops off very rapidly just outside the cloud chamber, some of the low energy particles that trip the counters will be deflected away. As a crude approximation one can say that the average curvature of a charged particle between counters is about 1/5 of that in the chamber. If we assumed all particles to be cut out when their average radii of curvature between the counters were less than 50 cm. (the distance between counters) one gets ρ = 10 cm. or about 1 Mev. as the lower limit of energy in the cloud chamber. From the curve it is plain that only a small percentage of those which would have stopped should be cut out.

The work of Rossi, Sands and Sard[19] gives additional information about the number stopping. They report, from counter measurements, that one out of every 2,000 mesotrons which pass through 10 cm. of lead, stops in an additional gram per square centimeter of a light element. This is slightly more than that calculated above for 32 cm. of lead, but

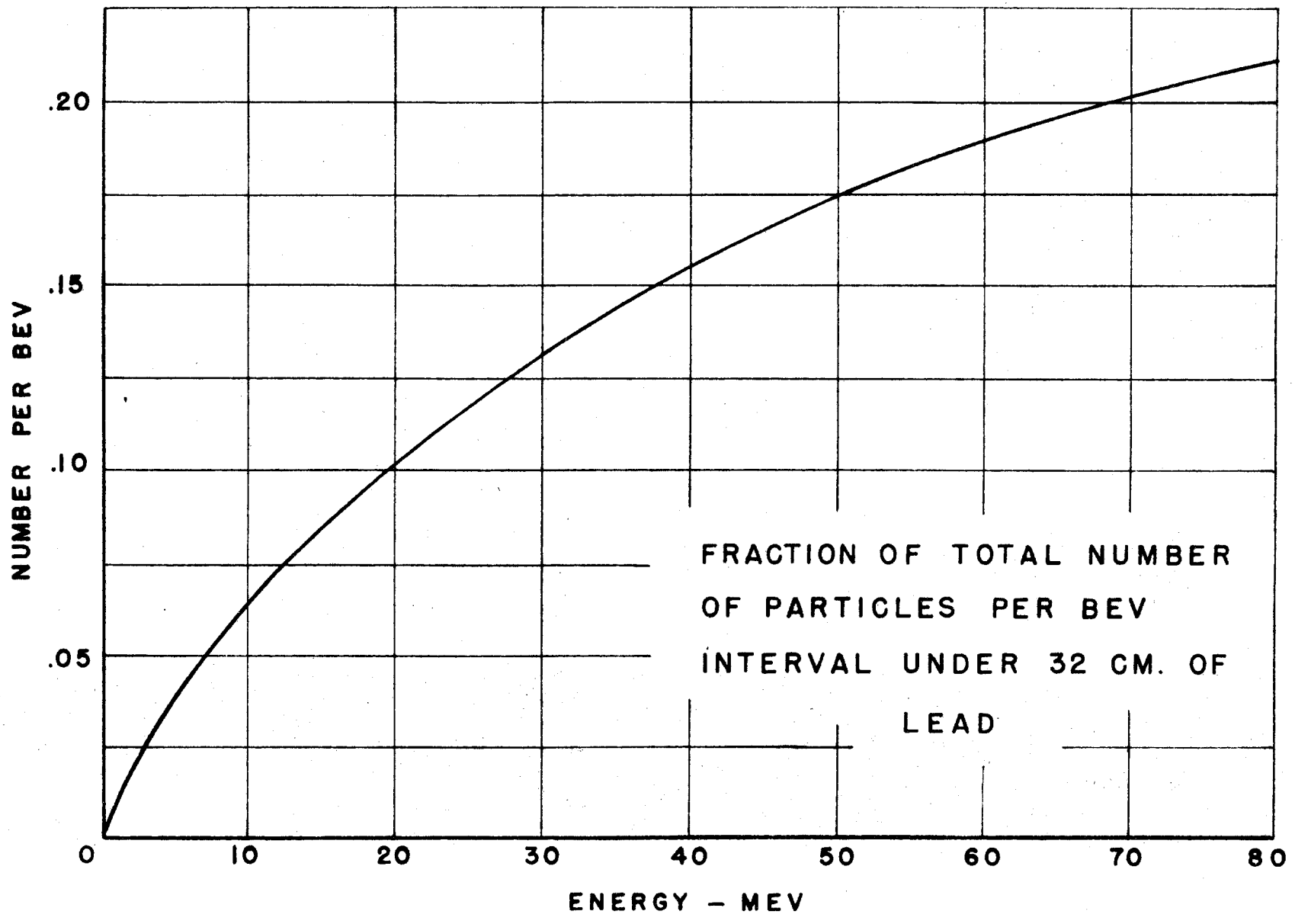
.20
.15
.10
.05
0
10
20
30
40
50
60
70
80
NUMBER PER BEV
ENERGY – MEV
FRACTION OF TOTAL NUMBER OF PARTICLES PER BEV INTERVAL UNDER 32 CM. OF LEAD

FIG. 16

both values are subject to considerable uncertainty. They also report that with no filter only one in 15,000 stops in a gm. per square centimeter. Thus, 10 cm. of lead seems to increase the number stopping by a factor of seven. 32 cm. increased it by roughly the same amount.

Summarizing, we find that in 7,000 pictures with an average of 1 traversal per picture, we should have found about seven stopping. We believe this estimate is uncertain by a factor of 2, since this is about the uncertainty in the various data presented. This value should be reduced appreciably because, although there is an average of one traversal of <u>any</u> plate per picture, most of the low energy mesotrons will only pass through the first plate before being deflected out by the magnetic field. A maximum correction due to this factor would be 3, but is probably less than 2. Thus, the number of mosotrons that should have stopped is not less than 1.2 and is probably about 3.5. Of these, all should have disintegrated because of the low atomic number of carbon.(20)

However, even though a mesotron disintegrates it may be mistaken for another event. For example, if the disintegration electron appears below the plate and the entering mesotron above, and there is no noticeable change in ionization, the event might be mistaken for an electron with an anomalous scattering. In fact, Fig. 2 could be interpreted as a mesotron of energy 7.5 Mev. entering from below and an electron of 88 Mev. emerging above, the secondary making an angle of about 10 degrees with the primary. In this the ionization density

however, would be 4.5 times the minumum and should be quite noticeable.* Similarly Fig. 10 could be interpreted as a low energy particle entering the bottom plate from above at the left of the picture and an electron of 28 Mev. leaving below. However, the low energy track does not appear to be ionized heavily enough for the apparent scattering and hence is quite likely an old track which is distorted, not scattered, and is probably not related to the 28 Mev. track. There were still other pictures that could have been interpreted as mesotrons stopping. The secondaries produced by them ranged in energy from about 15 to 30 Mev.

If the disintegration electron were emitted upwards from the plate and the mesotron entered from above, there would be no possibility of interpreting it as a scattered electron. The only other possibility is that it might be an electron pair, but the probability of a pair travelling upward is small. No such tracks were observed, however, even though one would expect 2 on the basis of the above calculations.

Several heavily ionizing tracks were observed, at least two of them mesotrons, but none gave rise to secondary electrons. The two slow mesotrons left the field of view before stopping. One case of a heavily ionizing particle was observed entering a plate from below with a lightly ionizing particle above moving in a direction about 10 degrees with that of the lower particle. This, however, could have been a mesotron entering from above, being slowed down and scattered in the plate. The energy lost was a factor of two too large for a mass 200

---

* The arguments as to probability do not apply here, since the particle, if a slow mesotron, does not pass through the lead.

mesotron, but the distortion was almost great enough to give this large an error (only a small portion of the upper track was visible). If a disintegration electron, its energy was 17 Mev.

The conclusions drawn from considerations such as these are:

1. Some of the mesotrons may have stopped, but none that were recognizable with any degree of certainty.

2. Since mesotron disintegrations are apparently quite rare phenomena, in a future experiment, an effort should be made to photograph only those events which are likely to be mesotron disintegrations. This might be done by using coincidence counters where one counter is delayed an amount equal to the mean life of the mesotron, i.e., tripped only by the disintegration electron. It could also be done with an anticoincidence counter to eliminate photographs of tracks passing through the entire cloud chamber.

3. In a future experiment, emphasis should be placed on eliminating distortion, and on using better photographic methods to enable an observer to easily distinguish heavily ionizing tracks. (see Section II)

4. The possibility of low energy particles being magnetically deflected out of the chamber should be minimized. A counter inside the chamber should do this. It should also increase greatly the solid angle subtended by the counters, thus increasing the coincidence rate. A deeper cloud chamber would also produce this effect.

BIBLIOGRAPHY

1. Leon Katz - Thesis - Calif. Inst. of Tech. (1943)
2. Biehl, Montgomery, Neher, Pickering and Roesch - Rev. Mod. Phys. 20, 353 (1948)
3. S. Korff - Electron and Nuclear Counters - Van Nostrand Company p. 65.
4. N. Bohr - Phil. Mag. 25, 10 (1913) 30, 581 (1915)
5. Møller - Ann. d Phys. - 14, 531 (1932)
6. H. Bethe - Zeit. f. Phys. 76, 293 (1932)
7. F. Bloch - Ann. d Phys. 16, 285 (1933)
8. Bhabha - Proc. Roy. Soc. 164, 257 (1937)
9. Heitler - Quantum Theory of Radiation - Oxford University Press, p. 219
10. Heitler - Quantum Theory of Radiation - Oxford University Press, p. 172
11. C. Anderson and S. Neddermeyer - Int. Conf. on Phys. London p. 121 (1934)
12. Turin and Crane - Phys. Rev. 52, 610 (1933)
13. Heitler - Quantum Theory of Radiation - Oxford University Press, p. 225
14. Heisenberg - Cosmic Radiation - Dover Publications, p. 75
15. Blackett - Proc. Roy. Soc. A 159 p. 1 (1937)
16. L. Le-Prince Ringuet - Sour. d. Phys. p. 207 (1937)
17. Jones - Rev. Mod. Phys. 11, p. 235 (1939)
18. Hughes - Phys. Rev. 57, p. 592 (1939)
19. Rossi, Sands and Sard - Phys. Rev. 72, p.120 (1947)
20. T. Sigurgierson and A. Yamakawa - Phys. Rev. 71, p. 319 (1947)